Novel Methods for Microfluidic Mixing and Control

Aschvin Bhagirath Chawan

Thesis submitted to the faculty of the Virginia Polytechnic Institute and State University in partial fulfillment of the requirements for the degree of

Master of Science
In
Engineering Mechanics

Ishwar K. Puri, Co-Chair

Sunghwan Jung, Co-Chair

Douglas P. Holmes

December 3, 2013
Blacksburg, Virginia

Keywords: microswimmers, microfluidics, mixing, valving

Novel Methods for Microfluidic Mixing and Control

Aschvin Bhagirath Chawan

ABSTRACT

Microfluidics is a constantly evolving area of research. The implementation of new technologies and fabrication processes offers novel methodologies to solve existing problems. There are currently a large number of established techniques to address issues associated with microscale mixing and valving. We present mixing and valving techniques that utilize simplified and inexpensive techniques.

The first technique addresses issues associated with microscale mixing. Exercising control over animal locomotion is well known in the macro world but in the micro-scale world, control requires more sophistication. We present a method to artificially magnetize microorganisms and use external permanent magnets to control their motion in a microfluidic device. This effectively tethers the microorganisms to a location in the channel and controls where mixing occurs. We use the bulk and ciliary motion of the microswimmers to generate shear flows, thus enhancing cross-stream mixing by supplementing diffusion. The device is similar to an active mixer but requires no external power sources or artificial actuators.

The second technique examines a methodology involving the integration of electroactive polymers into microfluidic devices. Under the influence of high applied voltages, electroactive polymers with fixed boundary conditions undergo out-of-plane deformation. We use this finding to create a valve capable blocking flow in microchannels. Electrolytic fluid solutions are used as electrodes to carry the voltage signal to the polymer surface. Currently we have demonstrated this methodology as a proof of concept, but aim to optimize our system to develop a robust microvalve technology.

For my parents and brother…

Acknowledgements

I would like to thank my advisor, Dr. Puri, for bringing me into the MuRG lab and ESM department. When I visited Virginia Tech for the first time, Dr. Puri welcomed me into his office and gave me an opportunity to pursue a graduate education.

I would like to thank my committee members, Dr. Douglas Holmes and Dr. Sunghwan Jung, for their constructive criticism and advice. I have lost count of how many times I have barged into their offices to ask for research help. I appreciate Dr. Jung's influence in developing Chapter 2 and Dr. Holmes's guidance throughout the work covered in Chapter 3.

I have the sincerest gratitude for Suvojit Ghosh and Saikat Jana. These individuals personally molded my experimental and analysis capabilities as a researcher. Saikat introduced me into the world of microscale locomotion and taught me the skills I needed to carry out my research. Suvojit helped me develop an analytical mind and taught me to think about problem solving from a fundamental perspective. Both of these individuals have always been critical of my work and I would not have been able to carry out the studies in this thesis without their guidance.

I extend a heartfelt thanks to Behrouz Tavakol, Ravi Kappiyoor, and Stephanie Roldan for helping me through this journey. To Behrouz, you have been a great colleague but also a great friend to work with. To Ravi, I have lost count of how many times you have helped me throughout my time at Tech. I cannot thank you enough for your programming expertise. To Stephanie, thank you for helping me with my work and being a pillar of support throughout this journey. To all of my friends who have given me support over these two years, I cannot thank you enough.

Finally, I want to thank my family. To my brother, thank you for always being supportive and a football buddy to talk to on weekends. To my mom and dad, thank you both for the opportunities you have given me throughout my life. You two have provided me with everything a son could ask for. You both have helped me become the person I am today. I am truly grateful to have parents as wonderful as you two.

Table of Contents

List of Figures

Chapter 1: Introduction

1.1 Challenges in Microfluidics

The control and manipulation of fluid flows at micron length scales, termed microfluidics [1, 2], has received recent attention as the increased availability of fabrication methods and integrated flow configurations have made it more readily accessible. The phenomena observed at this length scale have been well documented in areas such as biology [3] and colloidal science [4] nearly four decades prior. However, simple and effective man-made creation and manipulation of these flows remain a challenge.

Microfluidic systems are designed to exploit the fluid mechanics of laminar flows in small geometries [1, 5], reducing the cost, time, and infrastructure needed in comparison to macroscale analogs [6, 7]. For example, initial applications of microfluidic technologies were in analysis, due to the small quantities of samples and reagents needed to carry out chemical analyses with high resolution and sensitivity [2]. Today, microfluidic systems offer platforms for small-scale chemical, medical, and biological analyses [8]. One of the most developed microfluidics applications involves screening blood samples for protein crystallization [9]. This analysis technique tests for conditions such as pH and solute concentration [10]. Other state-of-the-art applications include, but are not limited to, high throughput screening for drug development [11], mass spectroscopy separations [12], and the production of polymer particles [13]. These systems have become highly sophisticated due to the development of constituent microscale system components.

Despite the vast literature available on microfluidic systems, manipulating microflows and utilizing the physics of the flow regime remain difficult [1]. Many of the analysis systems

mentioned earlier require integration of microfluidic components that demonstrate effective mixing, separation, detection, pumping, and valving. Mixing methodologies have been an active area of research in the past decade as a result of the low mass diffusion of liquids in laminar flows [14]. Microscale mixers, commonly known as micromixers have been implemented in many systems to overcome this challenge. Micromixers, have specific intrinsic advantages and disadvantages that must be tailored to applications [15]. Separation techniques rely on physiochemical properties such as charge, mass, and diffusivity for discrimination [16]. The increased interest in micro total analysis systems (μTAS) has led to the improvement of microscale separation functionalities [17]. Detection and sensing methods in microfluidic systems utilize small sample volumes while maintaining minute analyte detection [14]. Detection technique sensitivity must be suitable for a diverse range of analytes and possess the ability to be miniaturized. Electrochemical methods are common in sensing devices due to their ability to handle these challenges [18]. In macroscale pumping systems, pressure-driven flow is ubiquitous. Conversely, in microfluidic systems, the scaling effects associated with the area reduction make electrokinetic pumps (EKPs) more suitable for most applications [14]. Although EKPs provide pulse free flows, high voltages and electrochemical reactions at electrodes can create problems [19]. Additionally, microscale valves, commonly known as microvalves, need to fulfill many requirements: provide good seals, consume little energy, and create minimal dead volumes [20]. Different valve concepts possess strengths in one field or another [14]. In particular cases for the system components mentioned, miniature versions of macroscale analogs are suitable while other cases require new techniques. However, a complete review of the microfluidic system elements mentioned is too complex for this context. As such, in this thesis we focus primarily upon mixing and valving methodologies.

1.2 Introduction to Microfluidic Mixers

Flows in microfluidic systems have relatively low velocities in small channel dimensions resulting in low Reynolds numbers (Re). The Reynolds number is defined as:

$$\mathrm{Re} = \frac{\rho U D}{\mu}$$

where ρ is fluid density, U is fluid velocity, D is the channel dimension, and μ is the dynamic viscosity. The dimensionless Reynolds number characterizes flows. In microfluidic systems, this number is typically small, denoting laminar flows. The absence of turbulence makes the primary mode of mixing molecular diffusion [21]. The mixing time for a purely diffusion-driven scenario can be estimated from the following equation:

$$t_{mix} = \frac{w^2}{D}$$

In this equation, t_{mix} is the mixing time, w is the channel width (of the order of 100 μm), and D is the diffusion coefficient (of the order of 10^{-6} cm^2 s^{-1} for particular species) [22]. As a result, devices that only utilize diffusion require long mixing times and channel lengths [23].

Adjacent laminar streams in a microchannel mix through molecular diffusion at the shared fluidic interface [1]. Complete mixing in this setup requires a long channel and considerable time [15]. In order to reduce the axial length and time required for mixing, transverse flows must be generated [1]. Researchers employ active and passive methods to generate these shear flows [24]. Passive strategies rely on the interaction between the externally driven flow and channel geometry while active strategies rely on the interaction between the flow and external disturbances [15]. Another parameter to consider is the angle between inlet

channels for the fluid streams, but this factor has been shown to have no significant effect on mixing performance for either a passive or active mixer [25].

Passive mixers are designed for low Reynolds number flows [26]. Even though passive mixers do not require energy inputs [27], the geometrical structures needed to induce mixing are difficult to microfabricate and utilize complex processes such as photolithography [28]. It should be noted that designs capable of shear flow generation do not scale well with system size. The effectiveness of these mixers diminishes considerably with reduced geometries [29, 30]. Passive micromixers that generate laminar chaos in accessible geometries have been widely adapted to many applications. Popular designs include mixers with obliquely oriented grooves on channel walls [28, 29, 31], channels with zig-zag paths [27], and channels with 3D-serpentine designs [28, 29]. In addition to these designs with complex geometries, parallel and sequential lamination micromixers are also common [32, 33]. Lamination micromixers enhance mixing by increasing the contact surface area between adjacent streams through complex channel architecture. This architecture reduces the channel length and time required for complete mixing [1]. Many other passive strategies not mentioned here have also been widely adopted by researchers. Overall, passive methodologies are a popular choice for lab-on-a-chip systems, but require either complex fabrication techniques or complex channel designs [14].

Active mixers typically induce mixing by locally forcing fluid streams to increase interfacial area under complex control strategies [23]. Examples include magnetohydrodynamic mixers [34, 35], piezolelectric mixers [36], acoustic mixers [37], bubble mixers [22, 38], oscillating pressure mixers [39], electro-hydrodynamic mixers [40], and electrokinetic mixers [41]. The chosen mixer is dependent upon reagent type and the Reynolds number of the flow [23]. It should be noted that a complete review of micromixers is too complex for the scope of

this thesis. For more information on this subject, please consult the references provided at the end of the thesis.

Chapter 2 details a mixing method that possesses characteristics of both active and passive micromixers. The technique generates transverse flows without complicated sidewall channel geometry or channel architecture and does not require an energy input or complex control.

1.3 Introduction to Microfluidic Valves

The development and implementation of robust microvalve designs have helped successfully integrate microfluidic systems into industry. Flow regulation, on/off switching, and seal formation are the primary applications of microvalves [20]. Like micromixers, microvalves fall into two categories: active and passive. Active microvalves can use mechanical and non-mechanical parts and external systems for actuation. Similarly, passive microvalves can use mechanical and non-mechanical moving parts [20]. Active microvalves with mechanical moving parts and external actuation systems will be considered in this section.

Active microvalves with moving mechanical parts can utilize magnetic [17], electric [42], piezoelectric [43], thermal [44], or bistable [45] methodologies. Magnetic microvalves require considerable energy input, but permanent magnets can be integrated into these valves to reduce power consumption while increasing magnetic forces [44, 46]. Among magnetic microvalves, pinch-type valves that create seals by deforming tubing or channels are favored. These valves provide zero leakage flow, zero dead volume, fast response times, a high range of flows, and easy tubing replacement [20]. Electrostatic microvalves are primarily useful for regulating gas flows [47, 48]. These microvalves are made of conductive films sandwiched between flexible membranes [42, 49] or rigid silicone membranes [48, 50]. A voltage potential between two

electrodes causes the conductive film to move towards the electrodes to control flow, while the insulating layers prevent contact [51]. Piezoelectrics are known for producing large forces and small displacements at relatively high frequencies [20]. These materials are typically used for micropumps, but through hydraulic amplification piezoelectrics can be used as valves for liquid and gas flows [52]. Although these materials have fast response times, leakage flow rates produced by piezoelectric valves are comparatively high [53]. Thermal valves utilize thermal expansion properties of materials for actuation [20]. Although these valves are slow and consume considerable energy, thermal valves are simple in design and easy to implement [54]. Thermal valves such as bimetallic [44], thermopneumatic [55], and shape memory alloy [56, 57] valves produce large strokes and forces capable of controlling large pressure differences [58]. The active microvalves previously mentioned in this section require continuous power to operate whereas bistable microvalves only require power in a transient mode between two stable configurations [20]. Although these valves use minimal energy to thermally buckle membranes, bistable microvalves require complex fabrication techniques [45, 59].

Active microvalves with external actuation systems offer high pressure flow control with little to no leakage. Despite these advantages, external control systems are typically difficult to miniaturize [20]. Modular microvalves can have significantly different designs but have achieved success in industry by accommodating many samples in complex biological analysis techniques [60, 61]. Pneumatic microvalves use air pressure to control flow in microfluidic systems [20]. Initial valves were made from spin-coated PDMS layers [62], thin latex sheets [63], and micromachined silicon membranes [64]. A notable pneumatic microvalve operates by deforming a thin PDMS membrane into an in-line microchannel to pinch off fluid flow [20, 65]. This design utilizes cross-channel multilayer soft lithography processes to create the channel architecture

[65]. These pneumatic in-line microvalves have been used in μTAS enzymatic assays and polymerase chain reactions [66, 67]. External control systems effectively manipulate microchannel flow but require complicated equipment infrastructures, making portability difficult. A complete discussion of microvalves falls out of the context of this thesis. For more information please consult the references at the end of the thesis.

Chapter 3 describes a microvalve strategy that utilizes a similar mechanism for control as the externally actuated pneumatic microvalve, but uses electroactive polymers rather than air pressure to control flows. Our method requires less equipment than typical pneumatic microvalve designs.

1.4 Objective of Investigations

This thesis will focus on the implementation of microorganisms and electroactive polymers for flow manipulation at the microscale. Many studies have detailed the behavior and the fluid dynamics of propulsion for unicellular eukaryotes, but few have demonstrated sophisticated control over these organisms to achieve microscale tasks. Chapter 2 reports a study in which the swimming mechanics of paramecia in microchannels are used to induce cross-stream mixing without complex control methods. In addition to the challenge of effective micromixing, the implementation of operational microvalves is also difficult. Microvalves are a common feature of complex microfluidic systems, but the fabrication techniques and infrastructure needed to employ current microvalve designs are complex. Chapter 3 reports a study in which the out-of-plane deformation of electroactive polymers is used to regulate flow. These two projects discuss and propose simple solutions for challenges associated with microflows.

Chapter 2: Use of Microswimmers for Microfluidic Mixing

2.1 Introduction

The chemical, medical, and biological applications of microfluidic systems require effective mixing to perform necessary analyses [8]. However, small dimensions and low fluid velocities in microfluidic systems inhibit efficient mixing [1]. Micromixers employ active and passive strategies to supplement diffusion and reduce mixing times [24]. Active methodologies typically utilize external mechanical disturbances to perturb flows while passive methodologies utilize channel geometries and complex channel architectures to generate transverse flows to aid diffusion [15].

The control of microswimmers in mixing applications has not been fully explored. Gaining effective control over microorganisms can offer unique advantages in solving problems related to efficient microfluidic mixing. The ciliary motion of *Paramecium multimicronucleatum*, a ciliated protozoan, creates propulsion [68] and two micron sized vortices on either side of its body [69]. These observations have not been used to achieve microscale tasks. Previous studies have shown microorganisms to be controlled by chemotaxis, magnetotaxis, or galvanotaxis [70, 71]. Whereas chemotaxis is an inexpensive, passive control method [72], costly active control strategies have been utilized for magnetotaxis [71, 73] and galvanotaxis [71, 74]. Strong static magnetic fields (~ 3 Tesla) can align the swimming direction of microorganisms [75-78] but weaker static magnetic fields (~0.1 Tesla) appear to have no effect on the swimming behavior [79]. Active micromixers utilizing artificial cilia have demonstrated effective mixing but require costly control methods [80-82]. There is a push to develop a cost effective mixing strategy utilizing microswimmers with simple control strategies.

We hypothesize that we can efficiently use passive control methods to manipulate microswimmers to enhance microfluidic mixing. We artificially magnetize *P. multimicronucleatum* with magnetite nanoparticles (MNPs) coated in bovine serum albumin (BSA). Embedded permanent magnets in two different configurations fix the microswimmers' position relative to a Y-channel micromixer junction. We subsequently observe the effect the paramecia have on the two adjacent laminar streams in Poiseuille flow. The quantitative characterization of the mixing performance is given by the mixing index.

2.2 Experimental Methods

2.2.1 Culturing

The *P. multimicronucleatum* cultures were obtained from Carolina Biological Supply. The cultures were grown in a wheat seed (Carolina Biological Supply) and spring water solution. This solution was made by boiling wheat seeds at 300°C until the seeds cracked. Glass (Grainger, 60mm) and plastic (BioExpress, 60mm) petri dishes housed the cultures. Approximately 50 mL of boiled wheat seed solution and 1-2 cracked wheat seeds were poured into the petri dishes. The solution temperature was allowed to equilibrate to room conditions before paramecia were introduced.

When plating new cultures, old cultures passed through a 325 μm plastic mesh and were dispensed into microcentrifuge tubes (Grainger, 1mL). These tubes were subsequently centrifuged (300g, 12 minutes). The paramecia collected at the bottom of the microcentrifuge tubes. A VWR pipettor picked up 200 μL of concentrated paramecia from each tube and dispensed the contents into a petri dish. This process was repeated until all microcentrifuge tubes were centrifuged. The dish contents were then introduced into the new medium dishes. These dishes were kept at room temperature and out of direct sunlight. After 12 days, the cultures

peaked in population density and cell motility. This spike lasted until the 16th day. Based upon these findings new cultures were plated every 14 days.

The cultures were monitored daily. After 6-7 days, a biofilm would begin to form at the surface of the culture solution. Biofilms harm paramecia culture health as they cut off the oxygen supply to the microswimmers and allow anaerobic bacteria to flourish. A VWR pipettor was used to aspirate the culture medium and retard biofilm growth.

2.2.2 Experimental preparation of paramecia

Part of the procedure used to create new cultures was utilized. The cultures of interest passed through a 325 μm plastic mesh and were dispensed into microcentrifuge tubes. The tubes were centrifuged (300g, 12 minutes). From these tubes, 200 μL were dispensed into a petri dish for collection. After inspecting the contents of the dish for organism density, another round of centrifuging might be deemed necessary if the density was low. To prepare for the next round, the contents of the petri dish were dispensed into microcentrifuge tubes and the previous procedure was followed until the desired population density was reached.

These paramecia concentrations may contain debris, which has the potential to block channel inlets and perturb flow. It must be eliminated by a wash before paramecia are introduced into the device. Spring water was chosen as the washing medium. To wash a paramecia concentration, an equal volume of spring water is added to it and it undergoes the concentration process again. Another wash might be necessary if debris remains in the resultant concentration. Once free of debris, the paramecia solution can be used in experiments.

2.2.3 Fabricating PDMS microdevices

Soft lithography was used to make the microchannels. The first step to create the microchannels required constructing a detailed drawing of the design in AutoCAD using closed polylines. A Y-channel was chosen as the mixer design. Once complete, the drawing was sent out to Stanford Microfluidics, a third party vendor that made a mold from the drawing. The mold was made on a silicon wafer using photolithography. The silicon master (microchannel mold) has positive features representing the microchannel designs. These features are typically imprinted on a polymer substrate to make a microfluidic device.

The microchannels were created out of polydimethylsiloxane, PDMS (Sylgard 184, Dow Corning). A 10:1 mixture of PDMS, base to curing agent, was used. The PDMS components needed a thorough mixing to ensure crosslinking; a side effect of this process is bubble production in the mixture. In addition to preparing the PDMS mixture, the silicon master needed to be cleaned with isopropyl alcohol. Compressed air was used to dry the wafer before it was placed into a sterile petri dish (VWR, 150 mm). The PDMS mixture was poured over the wafer and the petri-dish was placed into a desiccator. The dish was then placed into an oven to bake at 65°C overnight. The dish contents were removed from the oven and the individual channels were cut out, punched (Harris Uni-core, 1.20), and irreversibly bonded to glass slides using a plasma cleaner (Harrick Plasma, PDC-32G). Although some of the initial microchannels were created in this manner, the paramecia-trapping microdevices contained permanent magnets and underwent a different construction procedure.

The microdevices that trapped paramecia contained either a set of permanent magnets or a single permanent magnet. The magnet(s) would tether the microswimmers at specific locations of the microchannel. The magnets used in this experiment were neodymium (NdFeB) grade N52

magnets (K&J Magnetics, 1/4 by 1/8 inch disk magnets). Two different magnetic orientations were employed in these experiments. One orientation, provided in Figure 2.1, involved a single magnet fixed over the portion of the microchannel immediately after the Y-channel junction. This orientation will subsequently be referred to as the flat magnet channel.

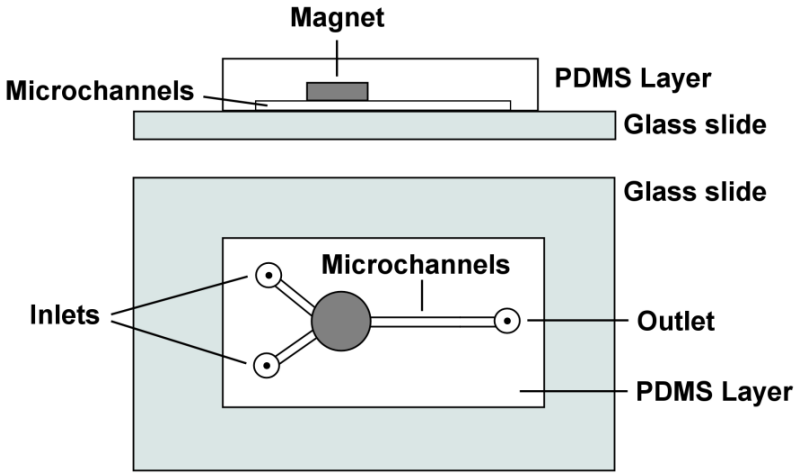

Figure 2.1: Side and top view of flat magnet channel. The blue background represents the glass slide while the white background represents the PDMS slab containing the magnet and microchannel. The magnet is represented by the gray rectangle in the side view and the gray circle in the top view. The circles at the inlets and outlets represent the holes punched into the PDMS slab to allow fluid flow to enter and exit the device.

The alternate magnet orientation consisted of two magnets separated by a thin slice of PDMS. The slices were cut from PDMS blocks at specific thicknesses using a vibrating microtome (Electron Microscopy Sciences). These magnet assemblies were fixed over the microchannel after Y-junction. By separating the magnets with a known thickness, the magnetic force experienced in the microchannel could be controlled. This orientation will subsequently be referred to as the magnetic sandwich channel. An example is provided in Figure 2.2.

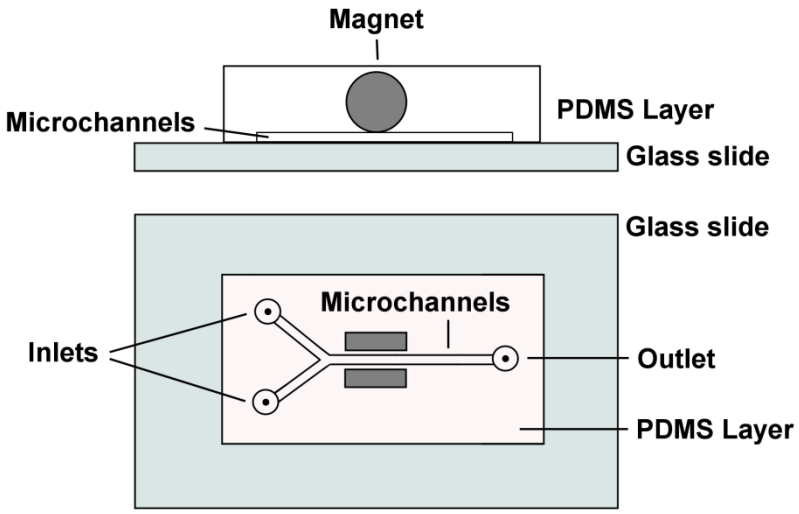

Figure 2.2: Side and top view of magnetic sandwich channel. The blue background represents the the glass slide while the white background represents the PDMS slab containing the magnets and microchannel. The magnets are represented as a gray circle in the side view and as gray rectangles in the top view. The circles at the inlets and outlets represent the holes punched into the PDMS slab to allow fluid flow to enter and exit the device.

The magnets used to make the flat and magnetic sandwich channels were held in place by additional magnets during the curing process to prevent the embedded magnet(s) from moving out of position.

2.2.4 Constructing the flat magnet channel

These devices were made in a two-step process. Following the protocol provided earlier, a 10:1 mixture of PDMS, base to curing agent, was prepared. The wafer was placed in a sterile petri dish (VWR, 150mm) after being cleaned. A thin layer of PDMS mixture was poured over the wafer. To ensure the distance between the magnet and the microchannel was kept consistent between fabrications, it was calculated that approximately 8.5 grams of PDMS mixture was needed to cover the wafer and translate the master's imprint to the polymer. Once the thin layer had been poured, the petri dish and its contents were put into a desiccator. Following desiccation, the dish was placed into an oven to bake at 65°C for 3 hours. The petri dish was subsequently

removed and another layer of PDMS mixture, totaling 22 grams, was poured over the wafer. The petri dish was then placed into a desiccator again to remove air bubbles. The dish was then removed from the desiccator and a magnet was placed flat side down into the uncured PDMS mixture. By placing another magnet on the bottom of the petri dish, we used magnetic attraction to move the embedded magnet to the specified location. Figure 2.3 depicts how we fixed the embedded magnet. For clarity, the magnet is shown fixed after the initial PDMS pour.

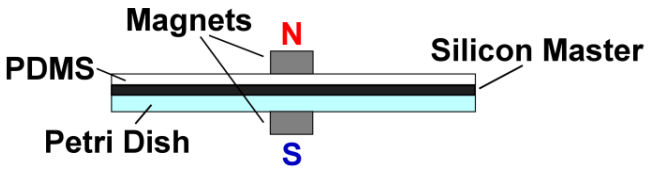

Figure 2.3: Magnet orientations for flat magnet channel during fabrication. The blue layer represents the petri dish; the black layer represents the silicon wafer; and the white layer represents the thin layer of PDMS over the silicon master. The magnets are represented by gray rectangles. The letters near the magnets represent the magnetic orientation of the magnets.

The petri dish and the magnet on the bottom of the dish were moved into an oven for a final bake at 65°C overnight. Leaving the bottom magnet in place ensured that the embedded magnet did not move while in the oven. After baking, the desired channels were cut out of the PDMS slab. Inlet and exit holes were punched and the microfluidic devices were irreversibly bonded to a glass slide using a plasma cleaner.

2.2.5 Constructing the magnetic sandwich channel

These devices were also made in a two-step process. The same protocol for the flat channel design can be followed with minor additions. For the final pour of PDMS, 33 grams of PDMS mixture was used to cover the magnetic sandwich and wafer. Fixing the position of the magnetic sandwich above the microchannel required the use of a combination of magnets or an axially long magnet to manipulate the sandwich. Figure 2.4 depicts the orientation of the

magnetic sandwich and the magnet used to fix the position of the sandwich. For clarity, the magnetic sandwich is shown fixed after the initial PDMS pour.

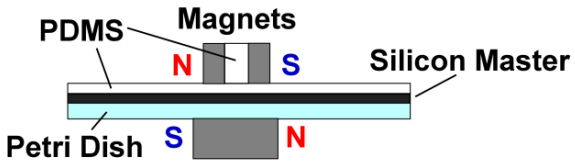

Figure 2.4: Magnet orientations for sandwich channel design during fabrication. The blue layer represents the petri dish; the black layer represents the silicon wafer; and the white layer represents the thin layer of PDMS over the silicon master. The magnets are represented by the gray rectangles. The letters near the magnets represent the magnetic orientation of the magnets in the sandwich channel microfluidic device.

2.2.6 Manufacturing magnetic nanoparticles

MNPs were synthesized and coated by a modified Massart coprecipitation [83] method and coated with BSA using a method adopted from the literature [84]. A 1:2 molar ratio of $FeCl_2 \cdot 4H_2O$ and $FeCl_3 \cdot 6H_2 0$, respectively, was dissolved in degassed and deionized water (ASTM Type II, LabChem Inc.) to form a 10.65% solute concentration by weight. The solution was then added to ammonium hydroxide to form a mixture with an 8.17% solute concentration by weight (salts to water and ammonium hydroxide). A black-brown precipitate of magnetite nanoparticles was formed. The mixture was centrifuged (5000g, 15 minutes) and the pellet was re-dispersed in deionized water to remove unreacted reagents and decrease the pH. The process was repeated 5 times. The MNPs were then pelleted again and re-dispersed in 5% (w/v) aqueous solution of BSA (Fisher BioReagents, Fraction V, heat shock treated). The dispersion was then sonicated for 1 hour using a probe sonicator (Fisher Sonic Dismembrator, Model 300). The resulting dispersion was a homogeneous reddish brown liquid when inspected at 400× magnification through an inverted microscope. The solution was made to stand overnight, then ultracentrifuged (Optima^{TM} L-90K, Beckman-Coulter) at 100,000g for 1 hour. The pellet was re-

dispersed in deionized water by sonication. This process removed excess BSA. The dispersion remained stable for several months when stored at 4ºC. The dispersion was characterized using DLS, nanoparticle tracking analysis (NTA, NanoSight) and TEM.

2.2.7 Experimental setup

The critical components of the experiment were a syringe pump, camera, inverted microscope, and microfluidic device. A schematic of the experiment is provided below in Figure 2.5.

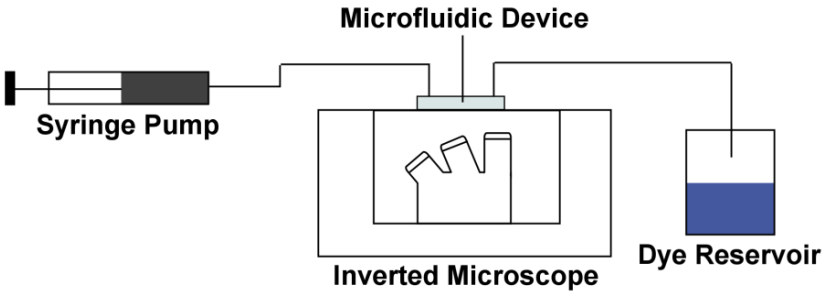

Figure 2.5: Experimental components. The blue rectangle on the inverted microscope represents the microfluidic device. The syringe pump drove flow through the microfluidic device into the reservoir. The dye reservoir was a beaker. The color of the liquid in the schematic is not representative of the actual color of the liquid exiting the microfluidic device. Not depicted is the camera used in the experiment. The camera was attached to the microscope to record images.

The syringe pump (NE-1400) depressed two syringe plungers (Henke Sass Wolf, 1mL) filled with food coloring. The colors chosen in this experiment were red and blue (Kroger). Another syringe filled with a concentrated paramecia and BSA coated MNP solution was connected to one of the food coloring syringes. This syringe was manually depressed to introduce paramecia into the flow during the experiment. The microscope (Olympus CKX41) focused images on the camera (Nikon D7000) sensor for capture.

The microfluidic device was placed on the microscope stage. The 4× and 10× objectives were used for imaging. The inlet tubes (Cole Parmer, #24 gauge) from the food coloring syringes were directly connected to the punched inlet holes of the microfluidic device. The same type of tubing ran from the device exit to the dye reservoir. The punched holes of the microfluidic

device were sized to fit the tubing. The microscope light intensity was kept relatively uniform during experiments. The phase contrast slider was set open.

A final paramecia concentration volume of approximately 0.8 mL was achieved by following the procedure to concentrate the paramecia. It was empirically determined that adding 5 µL of BSA coated MNP solution would sufficiently magnetize a majority of the paramecia for this volume. After introducing the nanoparticles, an incubation period of 25 minutes was deemed adequate for the paramecia to become artificially magnetized. To test for magnetization, a magnet was brought up to the edge of the petri dish containing the paramecia. If we observed a large number of paramecia travel to the magnet's position, sufficient magnetization had been achieved. Figure 2.6 contains images that depict paramecia with and without MNP internalization.

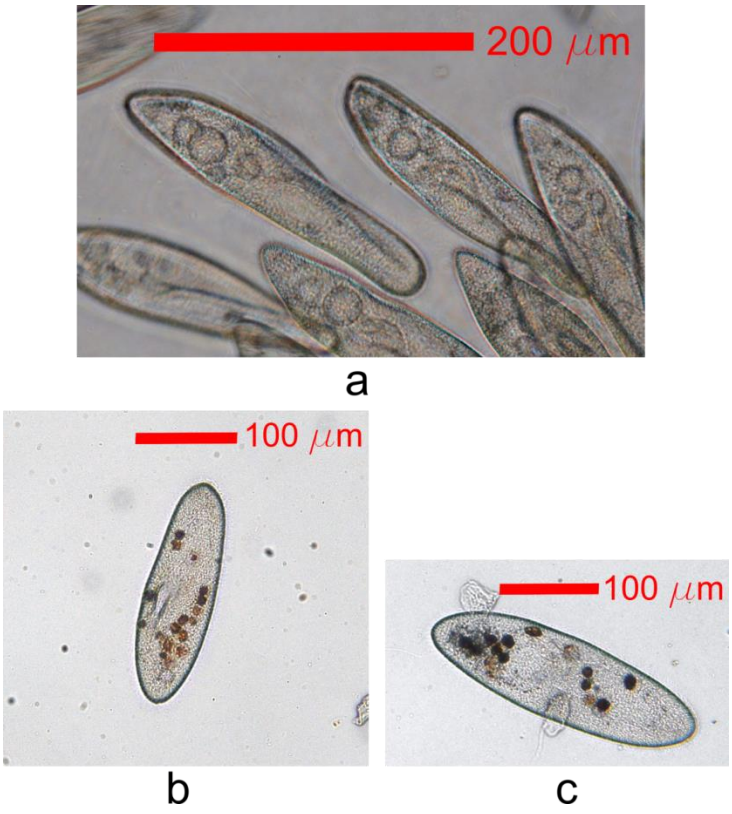

Figure 2.6: Paramecia with and without MNP internalization. (a) Optical micrograph of *P. multimicronucleatum* showing no MNP internalization. Due to the transparent nature of the microorganism, images can be obtained that depict internal components. (b) & (c) Optical micrographs of *P.*

multimicronucleatum with MNP internalization. (b) Depicts MNP organization after an external magnet has been applied. Application of an external magnet magnetizes the MNPs, enhancing the dipole strength of the nanoparticles. It is assumed that the dipole strength of the MNPs remains constant throughout the experiment. (c) Shows the randomness of nanoparticle agglomerations inside the microorganism before application of an external magnet. The exact mechanism of nanoparticle agglomerations and organization has not been investigated in this study.

The syringe pump operated on two syringes filled with food coloring. By specifying the syringe diameter, the flow rate through the microfluidic device could be accurately controlled. A wye connector (McMaster Carr, ID 1/16 inch) and tubing (McMaster Carr, ID 1/16 inch) connected a food coloring syringe with the paramecia and BSA coated MNP syringe. Tubing ran from the exit of the wye connector to another fitting (McMaster Carr, Luer Lock Tube Coupler) that attached to a needle (McMaster Carr, #24 gauge). A needle was attached directly to the other syringe in the pump. Tubing (Cole Parmer, #24 gauge) ran from both of these needles into the microfluidic device. Before connecting these tubes to the microfluidic device, the tubes were purged with food coloring to prevent air bubbles from entering the microchannels. After the inlet tubes were connected to the microfluidic device and once flow was established, the paramecia syringe was depressed to introduce the organisms into the device and the camera was used to record subsequent images. The images in Figure 2.7 show trapping of paramecia in the microchannels.

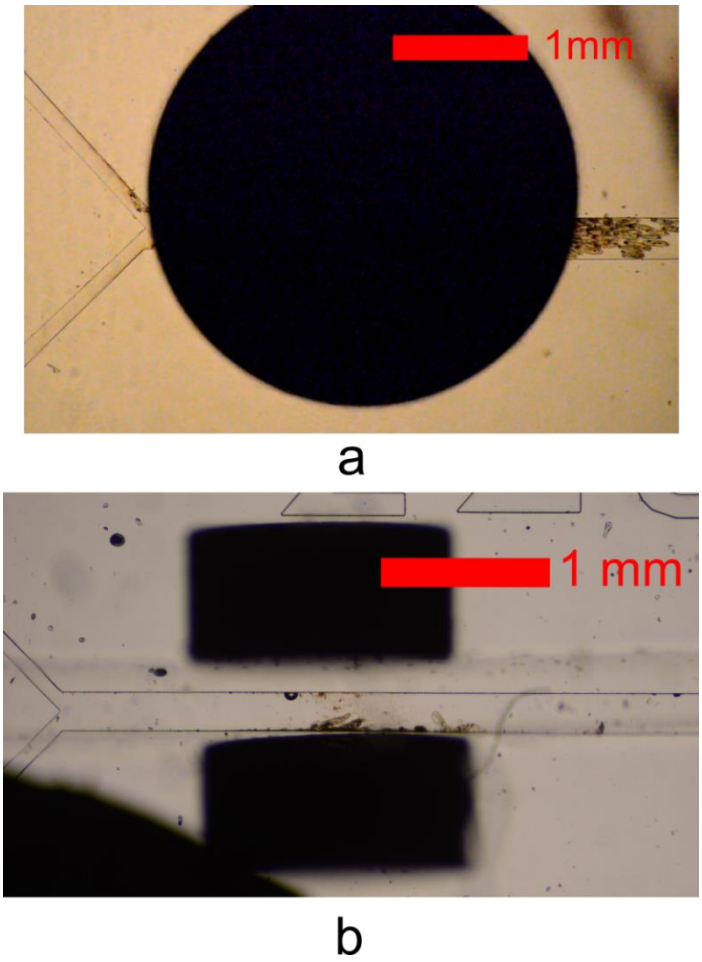

Figure 2.7: Tethering paramecia inside microfluidic devices. (a) The flat magnet orientation traps paramecia throughout the entire width of the microchannel. A drawback of this orientation is that it makes optical inspection under the magnet difficult. The trapping effectiveness of the flat magnet design is quite high given the number of paramecia that are attracted and tethered to the magnet. (b) The sandwich magnet orientation was able to trap paramecia on the walls of the microfluidic device. The magnets and channel widths between (a) and (b) are not the same size. These images were solely meant to show tethering using different magnetic orientations.

2.2.8 Determining food coloring diffusion coefficient, density, and color calibration

Using MATLAB, the diffusion coefficient was determined by calculating the maximum slope of the concentration profile at the interface of two food coloring streams along the axial length of the channel. The concentration profile is represented by:

$$C(x,t) = erfc\left(\frac{x}{2\sqrt{Dt}}\right)$$

where C is concentration, x is position along the channel cross section, D is the diffusion coefficient, and t is time. Taking the derivative of this function at the midpoint of the channel cross section yields:

$$\frac{d}{dx}C(x,t)\,|_{x=0} = \left.\frac{e^{\frac{-x^2}{4Dt}}}{\pi Dt}\right|_{x=0} = -\frac{1}{\sqrt{\pi Dt}}$$

Substituting time with distance down the channel, y, divided by average velocity of the flow, $\bar{V}$ yields :

$$t = y/\bar{V} \rightarrow \frac{d}{dx}C(x,t)\Big|_{x=0} = -\sqrt{\frac{\bar{V}}{\pi D}}\frac{1}{\sqrt{y}}$$

The maximum concentration gradient of each cross section along the channel is plotted and curve-fitted to $-\frac{1}{\sqrt{y}}$. The resulting coefficient of the fitted curve was used to determine the diffusion coefficient, since the average velocity is known. Figure 2.8 shows the fitted curve to the data taken from the calibration image. The calibration image was converted from an RGB colormap to an HSV colormap to preserve the color distribution along the channel. The maximum concentration gradient was calculated using these hue vales. The root mean square deviation from this fitting process is 0.1101. The magnitude of this value can be attributed to factors such as the calibration image quality, HSV to RGB conversion process, and statistical noise from the fitting calculations. From the fit, we determined the diffusion coefficient of the food coloring to be 2.1 x 10^{-5} cm^2/s. We determined the density of the food coloring to be 1155 kg/m^3 with a standard deviation of 8.223 x 10^{-5}.

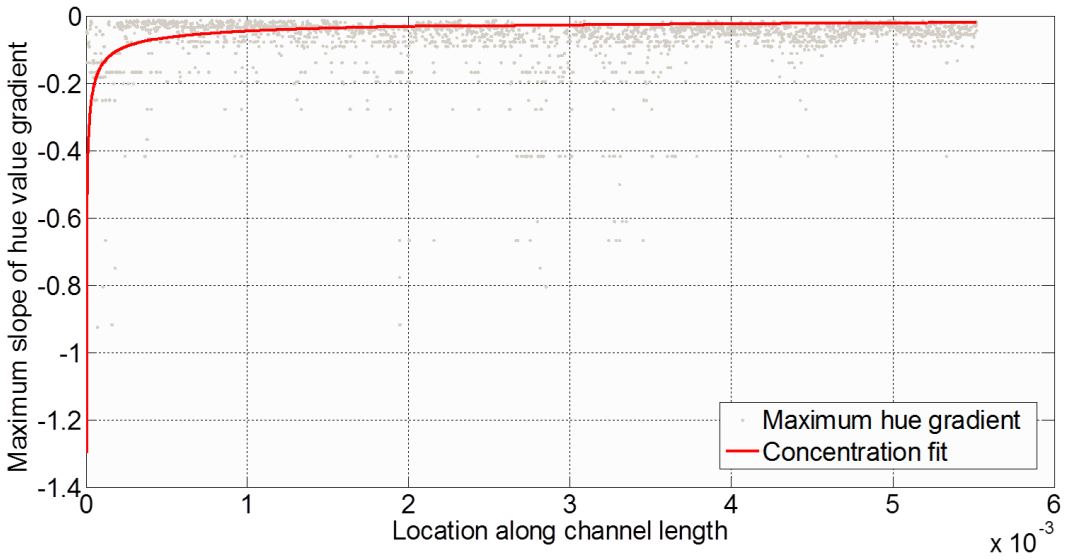

Figure 2.8: Curve fit to determine food coloring diffusion coefficient. The red line depicts the fitted equation while the gray points represent the maximum hue gradients taken at every cross section of the channel. Noise in the calibration image affected the fit. As given by the plot, the maximum slope of the hue gradient decreases along the length of the channel due to diffusion of the dyes into each other.

To further characterize the food coloring, we aimed to determine which dyes were most potent in affecting hue values. Ideally each dye would contribute an equal amount to the overall color. For instance, a vial filled with 50% red dye and 50% blue dye would result in purple. To observe the results associated with color potency, 11 samples of varying blue and red concentrations were prepared and vortex mixed. A 20 µL droplet from each sample was placed on a glass slide and examined under the microscope. In order to create a film of uniform thickness, two glass coverslips, 100 µm thick, were placed on either side of the drop. Another glass coverslip was placed on the other two coverslips to create a uniform 100 µm film. We chose a film thickness of 100 µm as the examination thickness because the microfluidic channels used in the experiment are 100 µm in height. Examining the sample at this height would provide us with an accurate representation of a color mixture we could experience in the experiment and the composition of that mixture. Figure 2.9 shows the plot of the color concentration calibration results as a function of varying quantities of blue food coloring. Yet again, the original RGB

colormap of these images was converted to an HSV colormap to identify colors. This plot was created with information extracted from the calibration images of the samples. The observations are not fitted with an equation. The line connecting the data points is meant to depict a trend between the resultant hue values and the concentration of blue dye in the sample. It appears that a mixture with a 20% concentration of blue or greater results in a hue value indicative of blue. The only concentrations that appear red are the sample concentrations where the percentage of blue dye is below 20%. Realistically, in a microchannel the minimum contribution of blue color we should experience is 50% if both inlet streams contribute equally to the flow in the main channel. If either color is diluted, the non-diluted color will be greater represented in the hue values. Given these results, mixed fluid in the microchannel should have a hue value closer to blue than red.

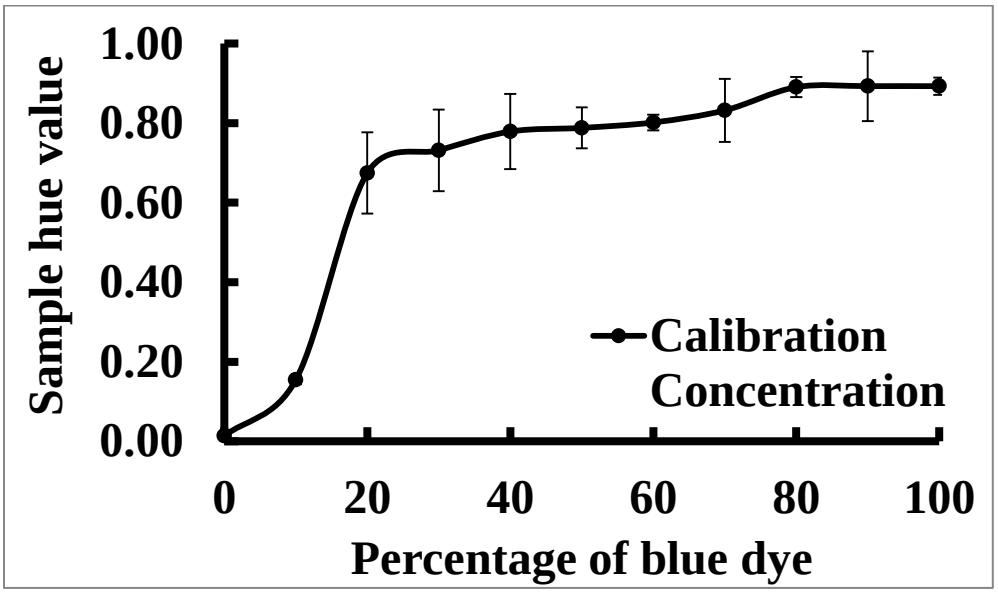

Figure 2.9: Calibration plot of food coloring samples. The plot shows the hue values of samples with varying concentration percentages of blue food coloring. Blue food coloring appeared to have a great effect on the resultant hue value of the sample. Hue values below 0.20 denote primarily red samples while hue values from 0.7 to 0.9 denote primarily blue samples. As given by the plot, any mixture concentration of blue above 20% yields a blue hue value.

2.2.9 Determining the Mixing Index

The mixing enhancement due to the presence paramecia was quantitatively characterized by calculating the mixing index (*M*) at spatially different cross sections in the microchannel. The mixing index formula from [85] was used:

$$M = \sqrt{\frac{1}{n}\left(\frac{I_i - I_m}{I_m}\right)^2}$$

where I_i represents the hue value at a given point along the channel width, I_m represents the average hue value of the cross section, and n represents the total number of sample points. Images were converted from an RGB colormap to an HSV colormap. An RGB colormap provides information regarding the amount of red, green, or blue in an image but does not clearly define the colors present in the image. For example, although an image may appear blue, the RGB components of that image can show that the blue color has substantial red and green components. In analysis, this colormap would incorrectly represent image data. Converting RGB values into HSV values distinguishes colors while also separating out saturation and brightness information. These HSV values would account for lighting changes and shadows thereby helping to discern color independent of brightness.

2.3 Results and Discussion

The two magnet configurations tested in this experiment to tether the paramecia were the flat magnet and magnetic sandwich orientations. We believe that the effectiveness of each configuration is dependent on the manner in which paramecia are fixed in the microchannel. The microchannel used for both cases has a width of 300 μm and a height of 100 μm. This channel geometry was chosen to due to the relative size of *P. multimicronucleatum*. We hypothesized that the channel width would have an effect on the mixing performance of the paramecia.

Channel widths substantially larger than the thickness of the paramecia would prevent microorganisms from effectively disturbing the flow. In this scenario, much of the flow could pass by the microswimmer unperturbed since the mixing capability of the paramecia is limited to areas adjacent to the cell body. The flow rate for both configurations was 20 μL/hr. The Reynolds number of the flow cannot be given since the viscosity of the food coloring is not known.

Experimental observations indicate the flow is laminar. It was empirically determined that a flow rate higher than 20 μL/hr washed away tethered paramecia while flow rates lower than this value cause pulsatile flow. For higher flow rates, we believe that the channel dimensions and flow rate lead to high local velocities that cause the fluid to exert a shear force on the microorganisms greater than the magnetic force between the magnet(s) and nanoparticle agglomerates inside the paramecia. An analysis between the strength of the magnetic and shear forces experienced by the paramecia in the microchannel was not carried out in this study. An experiment to quantify the magnetization of the microswimmers using Stokes' law was created, but this experiment required the deciliation of the microswimmers. Deciliation would ensure that the magnetic force experienced by a paramecium would primarily be influenced by the drag force of the cell body. This prevents the cilia from interfering with the magnetic attraction between the nanoparticle agglomerates and the magnet. Deciliation attempts were made but none were successful, therefore we were unable to characterize the level of magnetization achieved by the microswimmers.

The characterization of the flat channel design is shown in Figure 2.10. The purple lines denote where the hue profiles were calculated. The images depicting the flow in this figure represent flow scenarios that were dominant over the course of the image acquisition time

period. In order to get an accurate representation of the flow over time, we found it necessary to analyze a series of images to account for transient changes. These image series were recorded at different time steps separated by approximately 5 seconds.

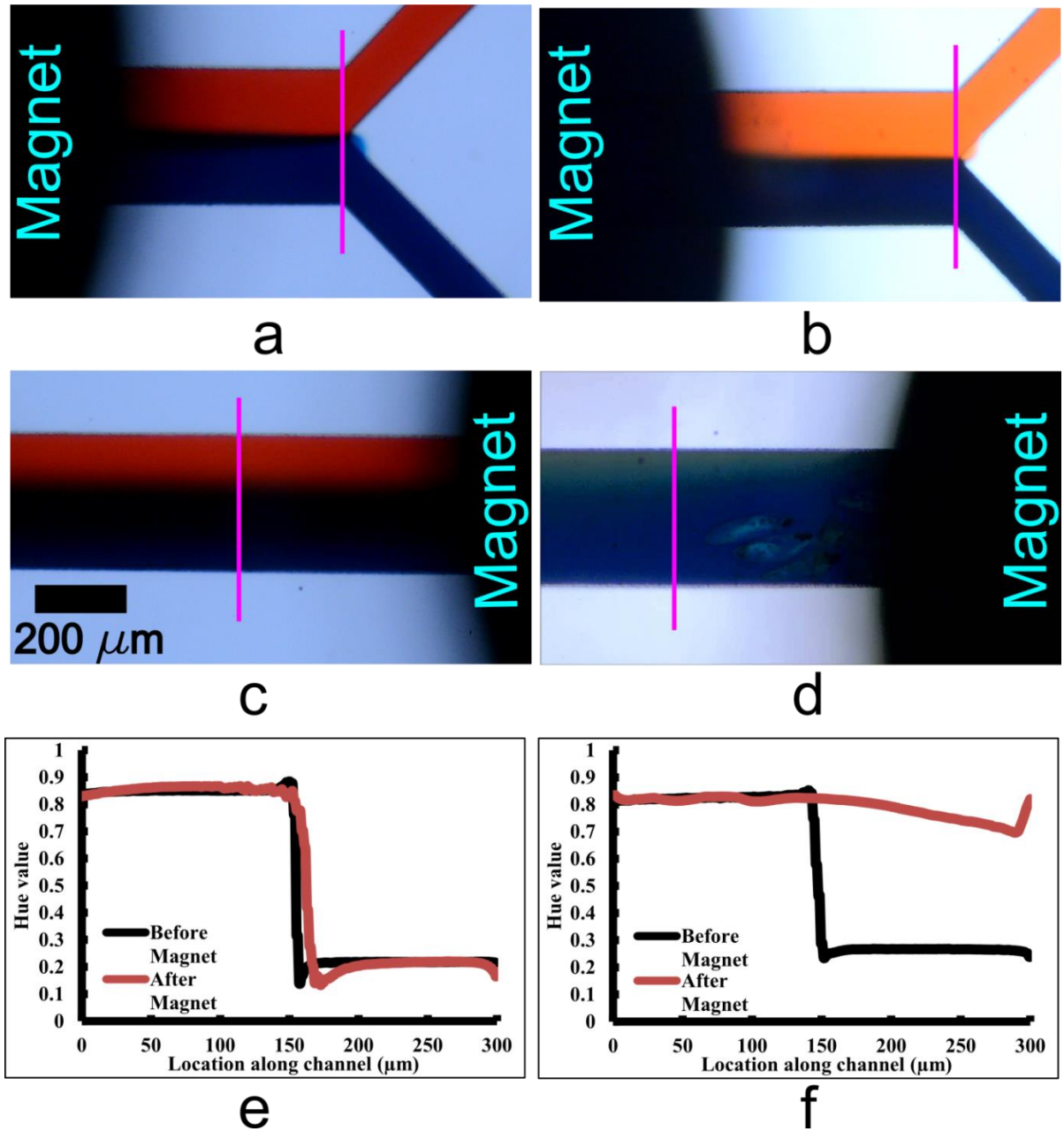

Figure 2.10: Flat Channel Characterization. The purple lines in (a-d) show cross sections where time averaged hue profiles were calculated in these 300 by 100 μm channels. The location of the cross sections was maintained between both test cases. The blue tint in the images was filtered out using a hue shift. (a) & (c) Optical micrographs depicting food coloring flows without the effect of paramecia. (b) & (d) Optical micrographs demonstrating the effect that paramecia in the flat magnet orientation have on the food coloring flow in the microchannel. The red food coloring in these images was diluted with the paramecia and magnetic nanoparticle solution obtained from paramecia concentration. (e) Shows the hue profile of (a) & (c). (f) Shows the hue profile of

(b) & (d). Given the results of the color calibration, a hue profile highly influenced by blue food coloring is expected and observed.

The control case involves no paramecia tethered in the microchannel. This scenario was chosen as the control case for both magnetic orientations because we wanted to demonstrate the mixing performance improvement between a diffusion driven mixing scheme and a paramecia influenced mixing scheme. In Figures 2.10(a&c), the food coloring pumped through the microchannel is mixed by diffusion at the fluidic interface. In (c) close to the channel walls, the colors remain the same as the respective inlet streams. The resulting hue plot, Figure 2.10(e), shows the difference in hue profiles before and after the magnet. We see that the profiles have relatively the same shape. These profiles represent the time averaged hue values at individual points along the width of the channel. The hue profiles of the cross sections before and after the magnet did not vary greatly with time as there were no perturbations in the microchannel. The hue profiles representing the flow before and after the magnet were calculated as an average of approximately 200 images, which comprised an image series. As mentioned before, the time between the image acquisition periods for the image series representing the flow before and after the magnet was approximately 5 seconds. This procedure provided data depicting the instantaneous influence of diffusion. This same time averaged protocol to generate the hue plot was also applied to the test case. From these results, we can see that diffusion at the fluid boundary does not adequately mix the fluids. The control case provides a basis for comparison for the test condition.

Figures 2.10(b&d) depict the test case in which paramecia were tethered in the microchannel under the influence of the flat magnet orientation. A qualitative comparison of the images representing the flow before and after the magnet highlights differences between the two. From these test case images, we observe that the fluid after the magnet appears substantially

more uniform in color than the fluid before the magnet. This color uniformity is a result of the perturbations from the paramecia which cause instantaneous mixing of the fluids in the channel. As mentioned earlier, the time between the two image series represented by (b&d) is short, thereby supporting this finding. Whereas the distinction between red and blue before the magnet is evident, that distinction is less clear after the magnet. We also observe the manner in which the paramecia are tethered in the microchannel. Figure 2.10(d) shows that paramecia are fixed on the channel wall and in the middle of the channel. Due to this positioning, we believe that the microorganisms are able to perturb the flow effectively since the microswimmers are spread throughout the channel width. Although it is not evident from the images, we observed that the paramecia were locally tethered to the magnet's location but the microswimmers maintained the ability to move along the width of the microchannel. The bulk and ciliary motion of the paramecia are what we believe to be the main factors for the difference in control and test case hue profiles. The specific location of the paramecia under the flat magnet is not very clear since the magnet partially blocks view of the channel. The Appendix provides images detailing the locations of paramecia in the flat magnet orientation by performing this experiment with fluorescent microparticles. Overall, this experiment reveals that paramecia perturb flow through cilary and bulk motion of the cell body.

Figure 2.10(f) shows that the hue profiles before and after the magnet do not have the same shape at specific locations across the channel width. As with the control case, these profiles represent the hue values over time at individual points along the width of the channel. The hue profile of the cross section before the magnet did not vary greatly with time as there was no perturbation at that location in the microchannel over time. The standard deviation of the time averaged hue values after the magnet is 0.037. As the standard deviation is an order of magnitude

below the reported values of the hue profile, a transient analysis of the hue profile for this case is not required. A comparison of the respective plots for the test and control case reveals that the hue profiles after the magnet are quantitatively different. The test case hue profile after the magnet appears to exhibit hue values typically found when analyzing blue substances. Recalling the color concentration calibration from the methods section, we note that even though the resultant color of the fluid after the magnet appears blue, it has been shown that any concentration of blue in the flow greater than 20% causes mixed fluid to exhibit blue hue values. The flow profile before the magnet in the test case clearly shows that the flow is equally composed of red and blue food coloring. Since the introduction of paramecia was the only parameter varied between control and test cases, we believe that the paramecia are responsible for the more uniform flow color after the magnet. Overall, the images appear to have a blue tint. This artifact of the images was resolved by implementing a hue shift in the analysis code. This allowed the hue values to correctly represent the color independent of blue tint. The light intensity was also taken into account in the RGB to HSV image conversion. The difference in color between the red food coloring in Figures 2.10(a&b) is due to color dilution as a result of connecting the paramecia and MNP syringe with the food coloring syringe.

The second section of the experiment examined the effectiveness of the magnetic sandwich orientation to tether paramecia in the microfluidic channel. A lower microscope magnification was chosen for this experiment to maintain consistent positions of the cross sections analyzed between the control and test cases. As mentioned before, we believe the manner in which the paramecia are trapped determines the ability of the paramecia to disturb the flow profile. Figure 2.11 characterizes the effectiveness of the magnetic sandwich orientation. As with the flat magnet cases, the images depicting the flow in this figure represent flow scenarios

that were dominant over the course of the image acquisition time period. To get an accurate representation of the flow over time, we found it necessary to analyze a series of images to account for transient changes. Approximately 10 images were analyzed for each case. Whereas the images used in the flat magnet case were extracted from a video, the images used in this case were images taken with a specific time delay. This image acquisition procedure reduced noise in analysis. The data used to calculate the hue plots was taken from image series of the control and test cases respectively. Since the image series contained both cross sections of interest, whatever mixing we observed occurred instantaneously.

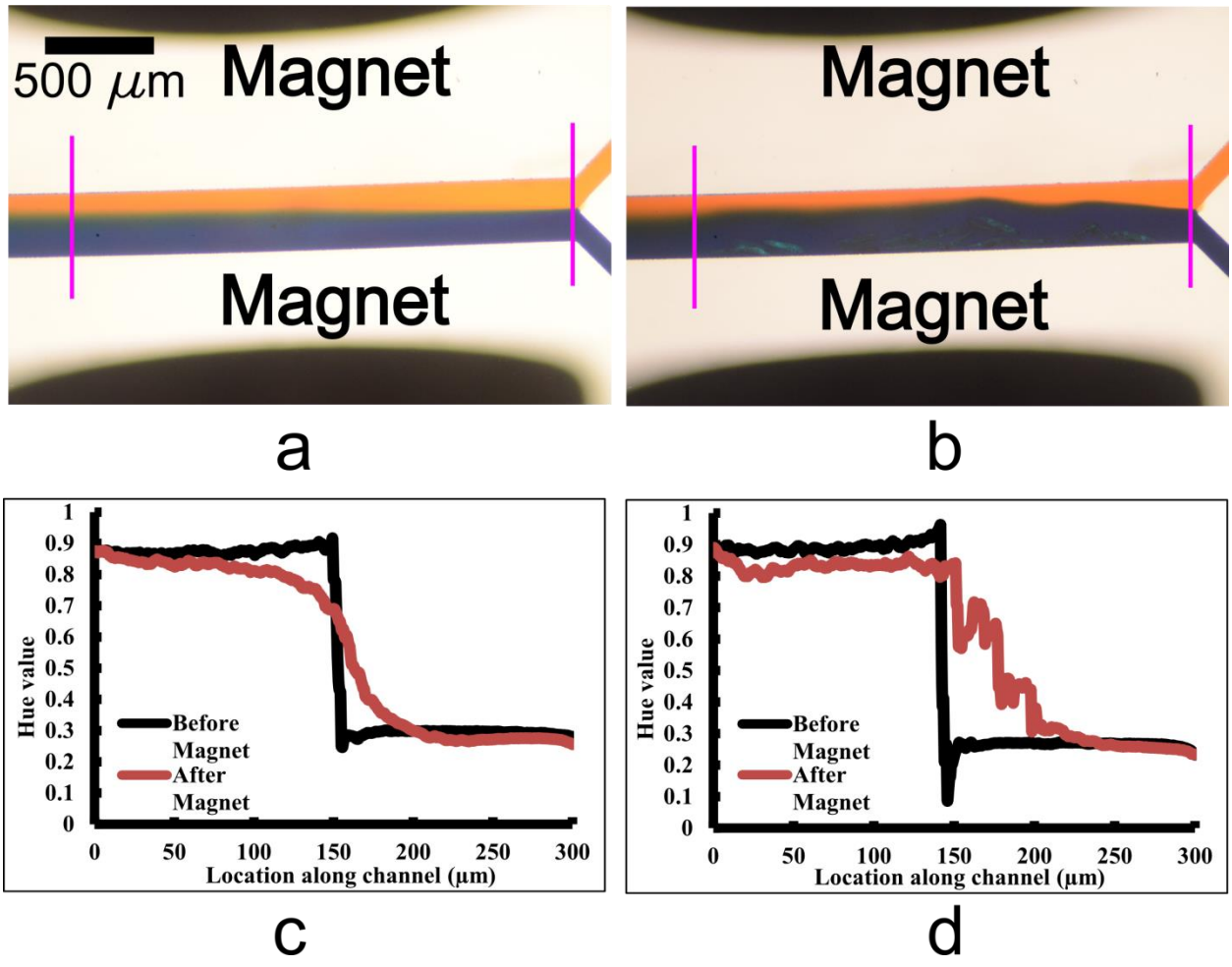

Figure 2.11: Magnetic Sandwich Channel Characterization. The purple lines in (a) & (b) show cross sections where hue profiles were calculated. The location of the cross sections was maintained between both test cases. (a) Optical micrograph shows food coloring flow in the microchannel without the influence of paramecia (b) Optical micrograph shows food coloring flow in the microchannel with the influence of paramecia. The red food coloring stream was diluted with paramecia and magnetic nanoparticle solution in both images. (c) Quantification of the effect of diffusion is given by the hue plot at the cross section

indicated in (a). (d) Quantification of the effect paramecia have on the channel flow is given by the hue plot at the cross section indicated in (b).

Figure 2.11(a) depicts the control case. As in the control case for flat channel orientation, we observe that diffusion at the boundary between the two fluids causes little mixing when examining the two cross sections of interest. The mixing achieved in this case is incomplete as only the fluid near the interface appears to be mixed while the fluid close to channel walls appears to be the same color as the respective inlet fluids. The resulting hue plot, Figure 2.11(c), shows the difference in hue profiles before and after the magnet. Although the line further down the channel length is not entirely after the magnets, this line was chosen because no paramecia were found to be tethered after this cross section during the experiment in the test case. These hue profiles appear to have different shapes, even though a qualitative examination of the fluids in the microchannel reveals only a slight difference in color. As with the flat channel control case, we see that diffusion at the fluid boundary does not adequately mix the fluids. This control case provides a basis for comparison for the test condition.

The test case in which paramecia were tethered using the magnetic sandwich orientation is given in Figure 2.11(b). A qualitative analysis of the flow before and after the sandwich shows that paramecia tethered in this manner do not effectively perturb the flow. The distinction between the red and blue fluids before the magnets becomes less clear further down the channel, but the separation is still evident. It is also important to note the manner in which the paramecia are tethered in the microchannel. This image shows that paramecia are primarily fixed on the channel wall near one of the magnets. We believe the higher magnetic gradient in that part of the channel, which is proportional to a higher magnetic force, is responsible for the microorganisms' positioning. This force pulls the paramecia towards the channel walls. The alignment of the magnetic sandwich in relation to the microchannel is difficult to manually coordinate. Even if

perfect alignment is achieved, the paramecia will experience stronger magnetic forces at the channel walls since the magnetic gradient is highest at the surface of the magnet.

The test case hue profiles at the cross sections of interest are shown in Figure 2.11(d). This plot confirms the qualitative findings. The hue profiles before and after the magnets do not have the same shape, but are similar enough to show that the flow has not been effectively perturbed. The hue profile after the magnets appears to have some artifacts of the flow before the magnets. A comparison of the respective plots for the test and control cases reveals that the hue profile after the magnets of the test case is quantitatively different than the analogous profile for the control case because it appears to exhibit greater mixing. The paramecia in this magnet orientation cause some mixing but this mixing is not significantly better than a flow that utilizes diffusion as the primary mode of mixing. Since the paramecia are fixed on the channel wall, it is hard for the microswimmers to perturb the fluid boundary and have a more pronounced mixing effect. In this scheme, the paramecia generate transverse flows primarily in the blue stream. Although these disturbances propagate to the red stream, the effects are not as great as in the flat magnet test case. The perturbations created by the microorganisms travel into the channel and into the channel wall. These shear flows in the magnetic sandwich test case must begin at one channel wall and propagate throughout the width of the channel. Those perturbations traveling into the wall do not have a substantial effect on the fluid flow. In the case of the flat magnet, the paramecia were tethered in the middle of the channel. This allowed perturbations to influence the fluid boundary and spread to the channel walls, disturbing streamlines in each fluid stream simultaneously. Conversely, paramecia in the magnetic sandwich orientation are fixed to the wall and have limited mobility. The microswimmers are not able to exert force on the flow through bulk motion as in the flat magnet test case since they primarily stay near the wall. This reduces

the effective amount of mixing the paramecia in the magnetic sandwich test case can perform. As in the flat magnet test case, the difference in color between the red food coloring in Figure 2.10(a) and Figures 2.11(a&b) results from the color dilution as a result of the connection between the red food coloring syringe and the paramecia and MNP solution syringe.

Several attempts to optimize the magnetic sandwich design were made, but most were ineffective at inducing significant mixing. Investigations into how well immobilized paramecia would cause mixing were undertaken. The results associated with this attempt show that immobilized paramecia were less effective at perturbing flow than non-immobilized paramecia. Similar to the magnetic sandwich test case, the paramecia in these investigations were fixed to the sidewall and were less successful than the paramecia in the magnetic sandwich test case at inducing mixing.

In comparing the flat magnet and magnetic sandwich test cases with the respective control cases, we see that the flat magnet orientation was more successful than the magnetic sandwich orientation at causing mixing. In the flat magnet test case, we see that the hue profiles before and after the magnet are fundamentally different, whereas in the magnetic sandwich test case the hue profiles before and after the magnets are distorted in some areas while maintaining the same general shape. A comparison of the hue profiles is not a substantial analysis to discriminate which strategy was more successful at mixing and therefore does not conclusively compare the control and test cases or the magnet configurations. To compare the effectiveness of the two configurations, we calculated the mixing indices associated with all cases reported. These results are provided in Figure 2.12. In Figure 2.12(a) a mixing index of 0.0 indicates that the fluids are completely mixed, while a mixing index of 1.0 represents no mixing. In Figure 2.12(b) a mixing index ratio of 1 indicates no mixing has occurred while an increasingly greater

mixing index ratio indicates a higher level of mixing. This ratio was computed by dividing the mixing index of the cross section before the magnet(s) by the mixing index of the cross section after the magnet(s).

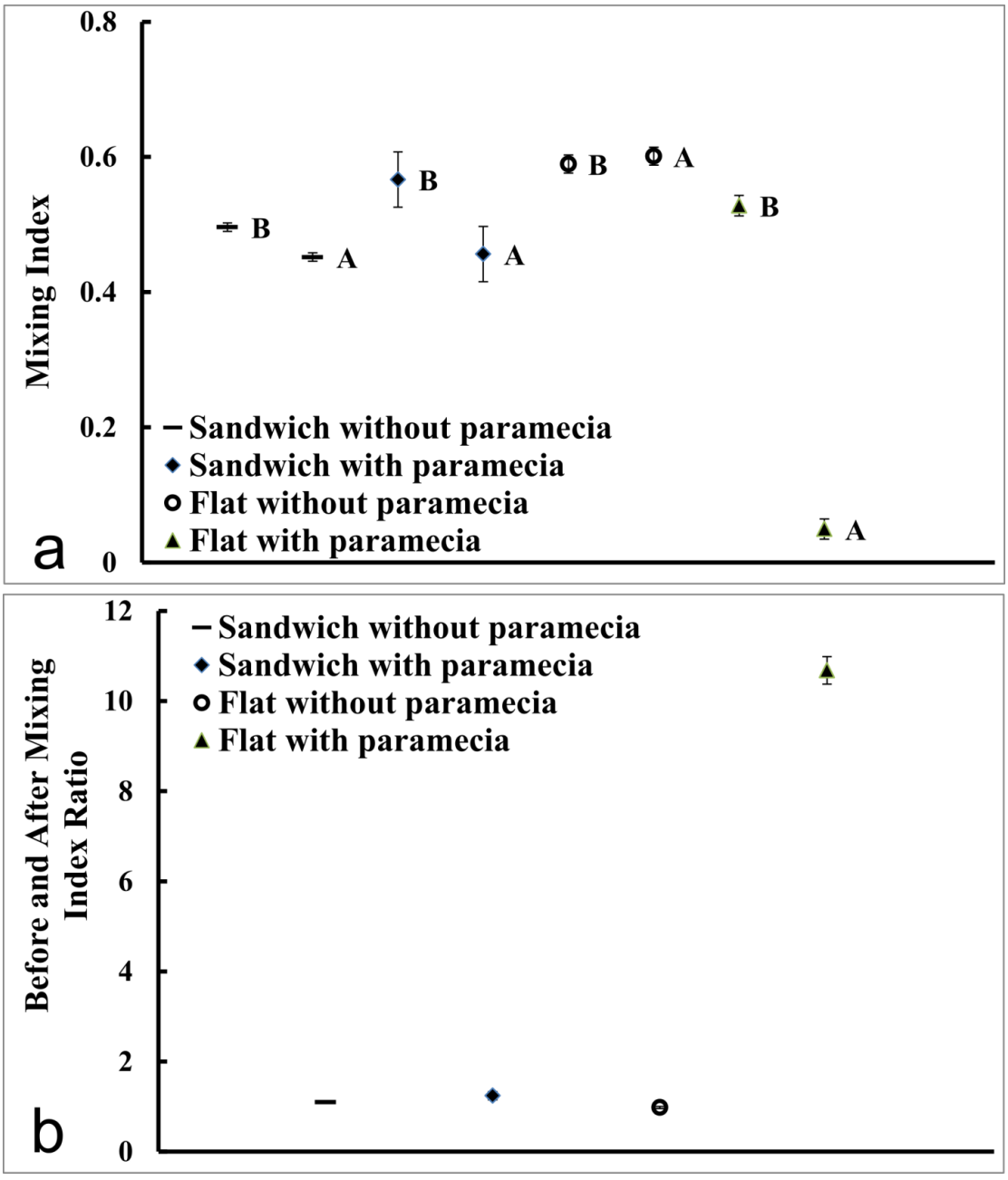

Figure 2.12: Mixing indices plot comparing cases. The calculated mixing indices reveal which magnet orientations were most effective at mixing the two food coloring streams. (a) B stands for before the magnet(s), and A stands for after the magnet(s). When comparing mixing indices, a value of 1.0 indicates no mixing while a value of 0.0 indicates complete mixing. Comparing the two cases with the magnetic sandwich channels, we see that the inclusion of paramecia did not significantly improve the mixing performance. Comparing the two cases with the flat magnet channels, we see that the inclusion of paramecia did have a significant effect on mixing performance. The flat magnet trapped paramecia in a manner which aided diffusion between the two

food coloring streams. (b) The ratio of mixing indices indicates the increased mixing performance for the flat and magnetic sandwich cases. A ratio near a value of 1 indicates that the mixing performance is marginal, while a mixing index increasingly higher than 1 indicates an increased effectiveness of magnetic scheme. The flat magnet channel with the inclusion of paramecia performs significantly better than the other magnetic configurations tested.

Figure 2.12(a) shows that the mixing performance of the magnetic sandwich channel is not as effective as the flat magnet channel. In examining the magnetic sandwich channel's control and test cases, we see that the mixing indices for the control and test case fall relatively in the same location along the mixing index axis, indicating that the inclusion of paramecia in this magnetic scheme improves mixing only marginally. This conclusion is confirmed by Figure 2.12(b) as the mixing index ratios for the control and test cases in this magnetic scheme result in a value of approximately unity. Since the paramecia were unable to effectively perturb the fluid boundary between the two streams or disturb flow using the bulk motion of cell bodies, the microswimmers were unable to thoroughly mix the food coloring streams. In examining the flat magnet channel's control and test cases, we see that the inclusion of paramecia in this magnetic scheme is very effective. The mixing index after the magnet is more than 5 times lower than the mixing index after the magnet in the control case. The flat magnet test case nearly achieves a mixing index of 0.0 which indicates a completely mixed fluid. This conclusion is confirmed by Figure 2.12(b). In this plot, we see that the ratio representing the flat magnet test case is significantly higher than the flat magnet control case since the mixing index after the magnet in the test case is lower than the mixing index before the magnet.

We hypothesize that the primary difference between these two magnetic schemes involves the strength of the magnetic force in the microchannel. We believe this factor influences how the paramecia are fixed in the channel. In the flat magnet case, the magnetic gradient is relatively uniform throughout the width of the microchannel since the magnet is a fixed distance away from the microchannel and the magnet surface is much larger than the channel width. This means that the force experienced in the channel is also relatively uniform. This uniform force

does not attract the paramecia to a particular part of the microchannel, but instead allows the paramecia to move locally within the region under that force.

In the magnetic sandwich case, the magnetic force in the microchannel is significantly different at the walls than at the channel center. Since the paramecia were artificially magnetized, the microswimmers were attracted to the stronger magnetic force at the channel walls. The presence of two magnets also increased the magnetic force experienced in the channel as compared to the one magnet used in the flat magnet orientation. In comparison to the flat magnet case, the magnetic force throughout the channel width and at channel walls in the magnetic sandwich case was higher. The more powerful and non-uniform magnetic force in the magnetic sandwich case prevented the paramecia from experiencing the mobility found in the flat magnet test case. This inability to move throughout the width of the channel impaired the microswimmers' ability to mix the two fluid streams because the bulk and ciliary motion of the microswimmer to induce mixing was inadequate in this instance.

2.4 Conclusions

We tested different magnet orientations to tether artificially magnetized *P. multimicronucleatum* in Poiseuille flow to induce mixing between two fluid streams in a microchannel. Of the two configurations we tested, the flat magnet orientation was most effective at inducing mixing. This mixing occurred instantaneously within our system. The microorganisms utilized ciliary and bulk motion to perturb fluid streamlines and generate transverse flows in this magnet orientation. Future studies looking to differentiate between the effects of ciliary and bulk motion on mixing should implement control cases in which the specific positions of paramecia are fixed in the microchannel. These fixed paramecia should not move in relation to the flow but would retain the ability to beat their cilia. This control case

would provide information regarding the dominant factor driving mixing by discriminating between these two types of motion.

In the flat magnet test case, the relatively uniform magnetic gradient throughout the width of the microchannel allowed the microswimmers to swim across the channel cross section. Tethered in this magnetic scheme, the paramecia disturbed the fluid boundary between the two fluid streams and created perturbations that propagated throughout the microchannel width. The flat magnet orientation is more than five times effective at inducing mixing than diffusion alone. The location of mixing can be controlled by fixing the magnets at different positions along the channel. To better visualize the experiment, fluorescent microparticles were used in conjunction with magnetic nanoparticles to track the position of the microorganisms, but this experiment resulted in cell death.

It should be noted that this application has limitations since it utilizes living organisms. This application is only effective for biocompatible fluids in a specific temperature and pH range. To prevent the presence of microorganisms in the mixed fluid, a filter must be connected to flow exiting the microfluidic device. Despite these limitations, the method we present utilizes simple and passive control strategies to manipulate microorganisms in a novel approach. With the increased amount of attention in the field of microbiorobots, this chapter's findings offer an uncomplicated control strategy that may be implemented in other studies to control microorganisms.

Chapter 3: Novel Microfluidic Valve using Electroactive Polymers

3.1 Introduction

Microfluidic analysis techniques perform chemical analyses more quickly and efficiently than macroscale analogs by using small quantities of samples and reagents while maintaining sensitivity and high resolution [2]. These microfluidic systems utilize microvalves to regulate flows and control reactions. Active microvalves with mechanical moving parts or external systems that serve as actuators require complex fabrication techniques and control methods [20].

The use of electroactive polymers (EAPs) as microvalves has not been fully explored. Microvalves are typically regulated by magnetic [17], electric [42], piezoelectric [43], thermal [44], and bistable [45] methodologies which utilize complex control. A popular alternative to these methods are pneumatic systems to control flows. Unfortunately, applied pressures lag behind control signals which hinder high speed valving applications [65]. Using EAPs as valves, however, would simplify fabrication protocols and allow for high speed applications. EAPs have been used in soft robotics [65, 86], lab-on-chip devices [87], energy harvesters [86], actuators [88], pumps [89], and sensors [88] but have not made a significant impact in microfluidics. Dielectric elastomers, a subset of EAPs which have been well characterized as actuators [88], offer good actuation pressures, theoretical efficiencies, and actuated strains in comparison to other high speed electrically actuated materials [90]. Currently, one of the greatest challenges for control over dielectric elastomers is the reduction of driving voltages [91, 92]. The development of a simple, low voltage, and cost effective microvalve would provide users with uncomplicated control methods.

We demonstrate a proof of concept methodology to use a common, well characterized dielectric elastomer, polydimethylsiloxane (PDMS), as a microvalve. We use an electrolytic fluid solution as an electrode. The solution bridges the gap between the wire electrodes and elastomer surface and requires less voltage than an analogous gel or solid conductor. This strategy maintains optical inspection of the channel and valve. When a PDMS film is exposed to an electric field, the film thickness reduces. Due to film incompressibility, the thickness reduction causes an increase in surface area. As the edges of the film are confined, this area increase results in out-of-plane deformation. When embedded in a microfluidic device, we can use this deformation to act as a microvalve and block channel flow. Only a high voltage power supply is needed to operate this system, greatly simplifying the control strategy.

3.2 Methods

3.2.1 Manufacturing the microfluidic device

The microfluidic device consists of two PDMS layers that sandwich a thin membrane. The molds used to make the microfluidic devices were made from plastic cutouts glued to glass slides. The plastic cutouts (Acrylonitrile butadiene styrene, ABS) were created using a laser cutter. The dimensions of the flow channel are larger than typical microchannel dimensions. A border on the glass slide prevents the PDMS mixture from spreading outside the area of the glass slide. Super glue bonded the border and plastic cutouts to the glass slide. Maintaining the spacing between the flow channel and actuation channel features is necessary to retain the channel geometry and architecture. Figure 3.1 provides an isometric, side, and top view of the microfluidic device design. The flow layer, a Y-channel design, in this figure sits on top of the actuation layer. In the actual device, these two layers are separated by a thin PDMS membrane. A model of this separation is shown in Figure 3.1(b). The two reservoirs under the inlet streams

were utilized in this experiment. The reservoirs in the main channel will be used in a future experiment.

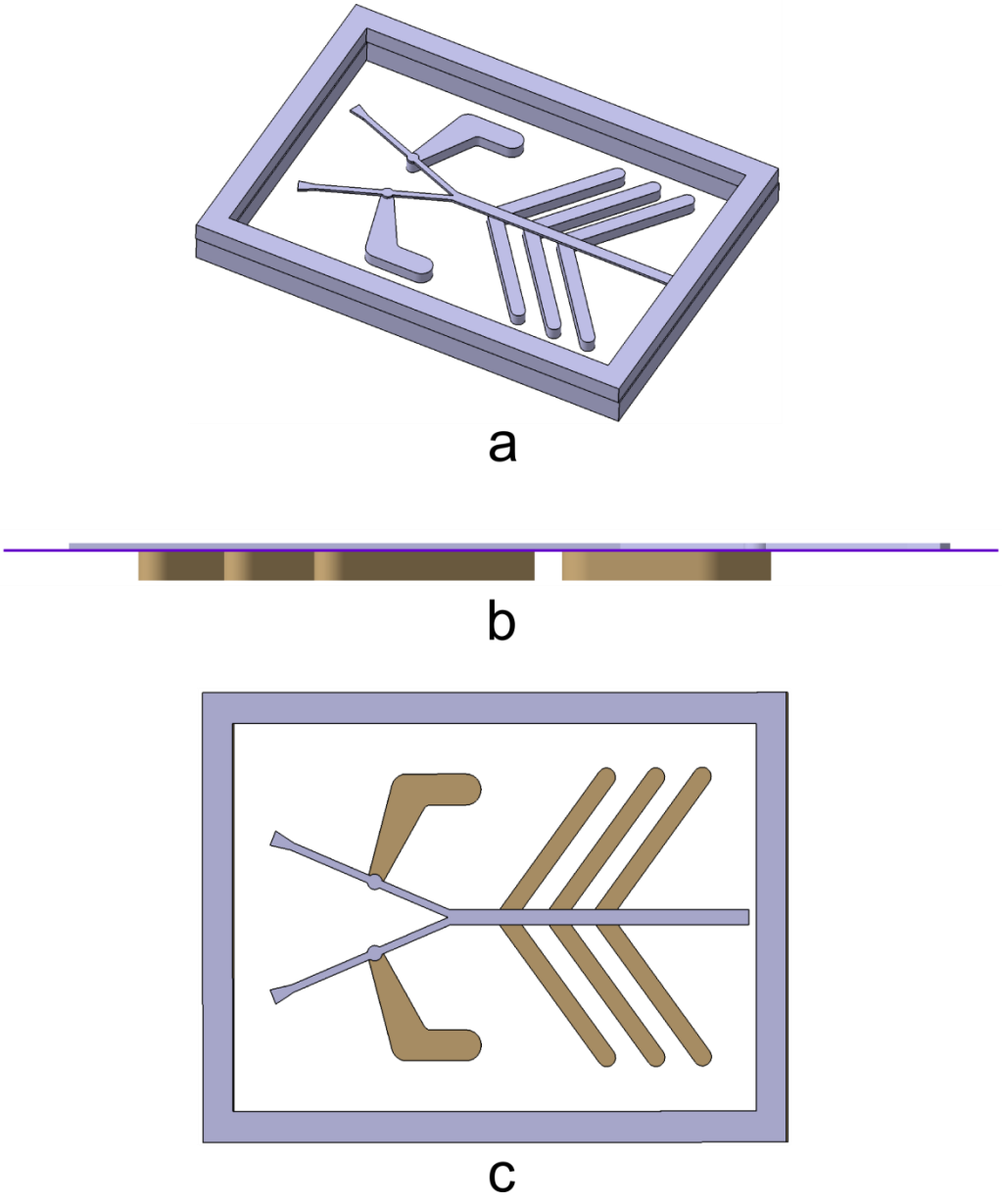

Figure 3.1: Schematics of microchannel with microvalve. (a) Isometric view of the flow layer and actuation layer. (b) Side view of the flow layer and actuation layer. The dark purple film between the two layers represents the thin film separating the microfluidic channel from the actuation reservoirs. (c) Top view of the flow layer and actuation layer. The flow layer contains a Y-shaped microchannel. The actuation layer contains reservoirs to hold the electrolytic fluid solution. The actuation layer lies under the flow layer.

PDMS (Sylgard 184, Dow Corning) was used to create the flow layer and actuation layer. A 10:1 mixture, base to curing agent, was prepared and poured into the molds. The molds were

desiccated to remove air bubbles created by the mixing process. Both molds were placed into an oven to bake for 1 hour at 90 °C. After the hour, the channel and actuation layers were extricated from the molds and a hole puncher (Harris Uni-core, 1.20) was used to punch inlets and outlets in the microfluidic device.

In order to create the thin film between the two layers a PDMS mixture, with the same proportions mentioned earlier, was prepared and deposited on an acrylic sheet. The sheet was then placed into a spin coater (Laurel Technologies Corporation Model WS-400BZ-6NPP/Lite). The sheet was rotated for 1 minute at 500 rpm, for another minute at 1000 rpm, and finally spun for 2 minutes at 1500 rpm. This order of spin times created thin films that were approximately 20 microns in thickness. The process to create these thin films has not been perfected. Once the process has become standardized we will attempt to match experimental results to theory since the buckling of the thin film is related to the film's thickness. The thin membranes were not baked, but allowed to cure at room temperature. The microfluidic device was assembled by bonding the thin membrane to the actuation layer and subsequently bonding the flow layer to the thin membrane. A corona treater (Electro-technic Products, Model BD-20AC) was used to treat the PDMS layers and films to be bonded. In some manufacturing attempts, the thin membrane bonded to the channel walls. A method to standardize bonding is being prepared.

3.2.2 Preparing the electrolytic fluid solution

The electrolytic fluid solution was created by dissolving sodium chloride in water and adding food coloring for visualization. The electrolyte solution is a 20% concentration by weight of sodium chloride (Spectrum S1240) in deionized water (LabChem, ASTM Type II). According to the literature [93], this weight concentration of sodium chloride creates a solution with a high conductivity which is adequate for its purpose within this experiment. After the sodium chloride

was added to the water, the entire solution was heated and then cooled to ensure solute dissolution. Solute residue in the solution impairs flow through the channel and future image analysis attempts to quantify microvalve effectiveness. Food coloring (Kroger) was added to the electrolytic solution to aid analysis and optical inspection. The inlet stream flows were different colors. The liquid in the reservoirs was not colored.

3.2.3 Experimental setup

Figure 3.2, provided below, details the components of the experiment. LabVIEW was used to coordinate the electrical inputs and image acquisition. The lines between experimental components represent connections. The line pointing to the microfluidic device is meant to indicate a system component and does not represent a connection. Not included in this schematic are the imaging components.

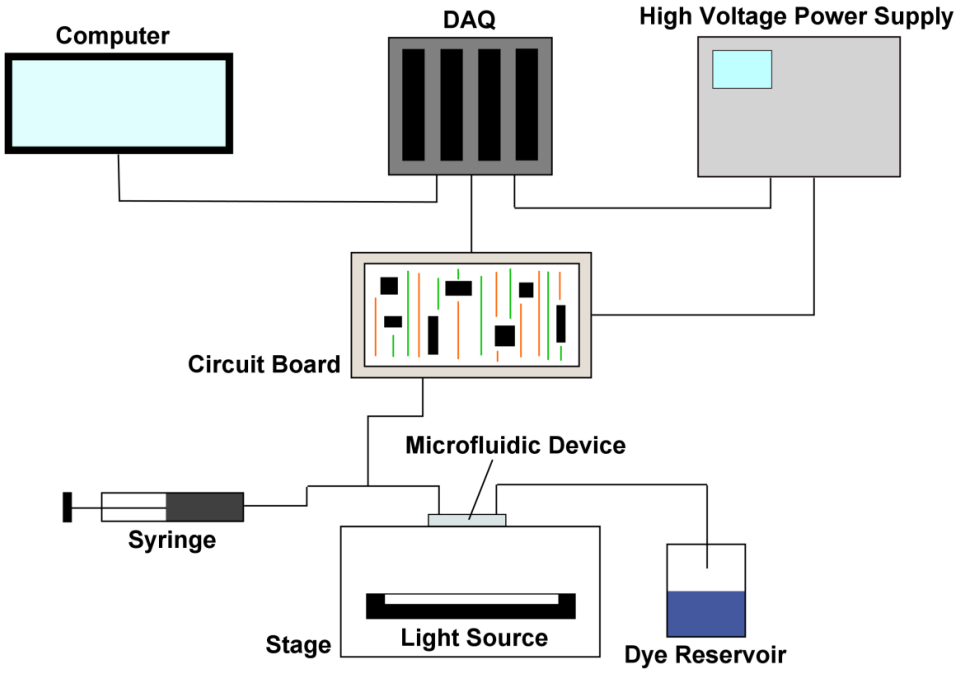

Figure 3.2: Experimental components. This schematic details the major components used. The lines between the components indicate connections. Signal generators from the LabVIEW computer software use the data acquisition system (DAQ) to coordinate the passage of the high voltage signal by controlling the circuit board components.

In order to coordinate image acquisition and signal transmission, a data acquisition system (NI CompactDAQ) was used. This device allowed the computer to send and receive data, allowing LabVIEW to control the experiment. LabVIEW uses signal generators to coordinate when the circuit board components allow the high voltage power supply (Trek 2300) signal to reach the microfluidic device's flow channel and actuation chambers. The signal from LabVIEW activates high voltage switches by means of an operational amplifier on the circuit board to allow the high voltage signal to pass through to the microfluidic device. Figure 3.3 details the components on the circuit board.

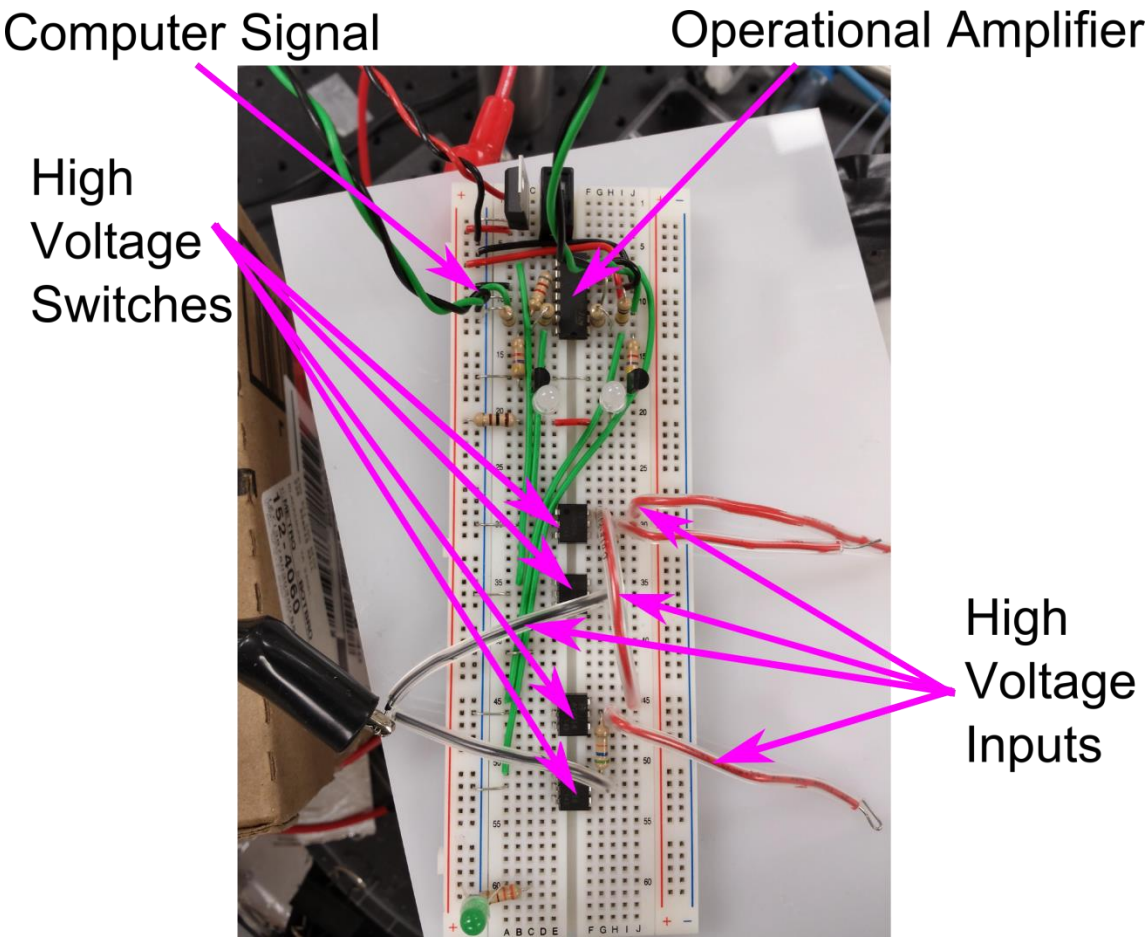

Figure 3.3: Circuit board components. The computer generated signals control an operational amplifier that provides low voltage signals to the activation terminals of the high voltage switches. Once activated, these high voltage switches allow high voltage signals from the high voltage power supply to pass through the circuit board to the electrolytic fluid solution in the microfluidic device's flow layer and actuation chambers.

These high voltage signals cause the thin membrane to buckle into the flow channel, thereby creating the valving effect we are trying to demonstrate. High frequency signals from the LabVIEW software were used to test the durability of the system and thin membrane. A light source is necessary to provide ample lighting for imaging. The stage is a transparent acrylic sheet. Spacers between the stage and light source allow light intensity to be customized. The stage is on a manually controlled linear stage to allow the focal distance between the lens and the microfluidic device to be adjusted. A camera (EO-1312C 1/1.8" CMOS Color GigE Camera) was used to capture images for analysis.

Poiseuille flow, implemented by a gravity driven system, passes through the microfluidic device into the dye reservoir. A gravity driven system was chosen to avoid the possibility of excessive pressure building up in the flow channel. For example a syringe pump might inhibit the performance of the thin membrane by leading to a pressure buildup, affecting film buckling. Syringes (BD Plastics, 10 mL) were filled with the electrolytic fluid solution and the plunger seals were punctured by needles to allow air pressure to drive flow. Valves were connected to the needles to allow air pressure to drive the system or restore original syringe function. Fluid from the syringe flowed into the tubing (Cole Parmer, #24 gauge) then into the device and exited to the dye reservoir. Although flow irregularities can exist with gravity driven systems, if the system is given enough time to equilibrate, the irregularities disappear. Due to the sensitivity of the gravity driven system, the stage was reinforced with springs to dampen vibrations from other lab equipment.

3.3 Proof of Concept

A schematic detailing the how the thin film buckles is provided in Figure 3.4.

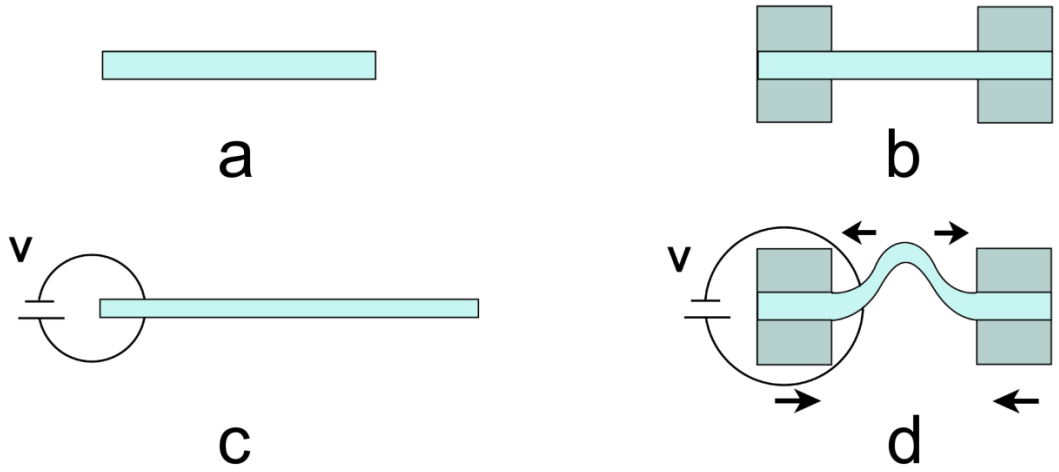

Figure 3.4: Explanation of valving mechanism. (a) A dielectric elastomer thin film with no applied voltage and no edge confinements. (b) A dielectric elastomer thin film geometrically confined with no voltage applied. (c) A dielectric elastomer thin film with no geometrical confinements undergoes an area expansion and thickness reduction when exposed to a voltage potential on its surfaces. (d) A dielectric elastomer thin film with edge confinements undergoes buckling when under an applied voltage. This out-of-plane deformation is what causes the valving mechanism in this study. The arrows indicate that the material wants to expand, but is confined by the boundary conditions. The interaction between these forces results in out-of-plane deformation. Shown in this figure is a 2D representation of the voltage induced deformation. The voltage range causing this deformation is on the order of kilovolts.

A comparison of Figures 3.4(a&c) demonstrates that a geometrically unconfined dielectric elastomer thin film experiences an area increase and thickness reduction under a high voltage signal. The thickness of the film reduces during this surface area expansion as a result of the incompressibility of the polymer. Conversely Figures 3.4(b&d) demonstrate a scenario in which the edges of the thin film are confined when voltage is applied. Figure 3.4(b) shows how we have fixed the thin film in our experiment. When we apply voltage to the thin film confined in this manner, compressive stresses form in the material as a result of the interaction between the fixed boundary conditions and radial strain. The dielectric elastomer undergoes the same thickness reduction and area expansion shown in (c), but the interaction mentioned previously causes the thin film to deform out-of-plane while experiencing these changes. This buckling phenomenon is the mechanism we utilize in our device. By embedding this mechanism in a microfluidic device, we can use voltage induced buckling to function as a microvalve and block

channel flow. Given this explanation of the valving mechanism, the functionality of the microvalve is demonstrated in Figure 3.5.

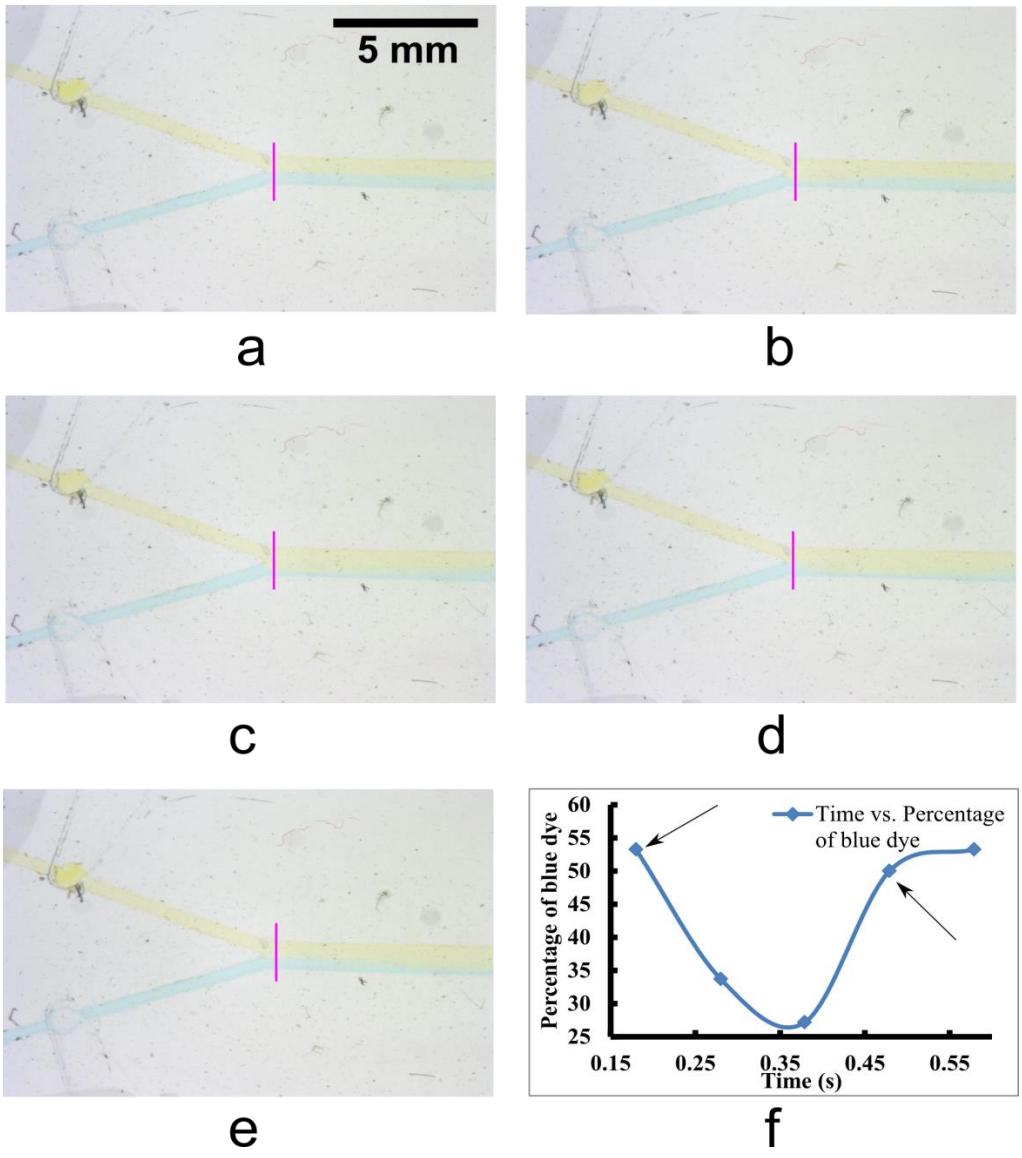

Figure 3.5: EAP valving performance. Images (a-e) show the microvalve and microchannel at time steps separated by 0.1 seconds. The microvalve controlling the blue inlet is activated. Looking at the evolution of the flow, we see that the blue food coloring flow is reduced in the channel over time. The segment of the inlet channel under the influence of the thin PDMS membrane is blocked and flow is not allowed to enter the main channel. This blockage is a result of the thin film buckling into the flow channel. The signal sent to the thin film that caused this buckling was a 1.3 kV signal at 1 Hz. (f) This plot shows the percentage of blue dye in the channel from (a-e) over time. We see that the blue-colored flow is reduced to nearly half its value when the valve was not activated. The arrows indicate when the valve was activated and deactivated, respectively.

Images (a-e) show the evolution of the flow over time in 0.1 second time steps. The magnitude and frequency of the high voltage signal sent to the thin PDMS membrane is 1.3 kV

and 1 Hz, respectively. Given this frequency, a duty cycle of 50% is expected, which means that the valve should be active for 0.5 seconds and inactive for 0.5 seconds. Ideally we should see the representation of blue fluid in the channel decrease over that same 0.5 second window. Given the time required for the fluid to flow from the valve to the cross section of interest, we should experience a time lag between the duty cycle and valve actuation period. The time lag is a feature of the system that we plan to investigate in future work. In Figure 3.5(a) we initially see that the flow in the main channel is roughly composed of equal streams of blue and yellow fluid. As time passes, the valve in the blue fluid stream is activated, and the thin film separating the microchannel and actuation reservoir undergoes buckling thereby blocking flow from the inlet supplying blue fluid. This allows the main channel to become filled with yellow fluid. After the active time period, we see the restoration of blue fluid flow in the main channel. These images provide information regarding the blue fluid decrease in the main channel.

In addition to the qualitative analysis, Figure 3.5(f) provides a quantitative analysis of flow in the fluid. This plot shows the percentage of blue fluid in the flow across the channel width at a location specified by the purple lines in images (a-e). These percentages are plotted as a function of time. The arrows indicate the period of time in which the valve is active and subsequently inactive. Each point along the curve represents data extracted from the images (a-e), respectively. Error bars could not be included in this image since this plot is generated from one data set. We currently do not have data sets that we can use to serve as a model of comparison to derive a statistical representation of the effectiveness of the system.

We are able to see that the microvalve is able to reduce the blue fluid flow in the main channel by nearly half over the time in which this system was investigated. The high voltage signal is sent to the system at approximately at 0 seconds, but we see that the system response

lags behind this input. This finding is in agreement with our earlier prediction. We currently do not have data characterizing the leakage flow rate and cannot compare the effectiveness of this system to previously established microvalves in the microfluidics field. More data characterizing the system is required to investigate the magnitude of the time lag. In addition, we have yet to quantify parameters such as the thin membrane's stiffness, permittivity of the dielectric film, thickness of the film, and applied voltage to match these experimental observations with established theory describing out-of-plane deformation of electroactive polymers. Finally, a high voltage monitor needs to be implemented to accurately gauge the voltage being sent to the thin membrane.

3.4 Conclusions

The microvalve design we have proposed appears to be an effective means of controlling gravity driven Poiseuille flow. We have not experimented with pressure driven flow generated by a syringe pump due to the potential of pressure build up in the microchannel impairing thin membrane deformation. Although only a high voltage power supply is needed, there are limitations to the design. Fluids in the flow and actuation channels need to contain a strong concentration of electrolytes to act as electrodes on the thin film. Furthermore, voltage concentrations at the confined edges of the thin film lead to breakages. These drawbacks will be considered as this project moves forward and is optimized. An advantage of this system stems from using conductive fluids as electrodes. Fluids are much more compliant than gels or solids allowing the dielectric film to undergo greater deformation at lower voltages. The energy consumption associated with this system is reduced while the reliability is improved since the fluids used in this experiment require voltages lower than the breakdown voltages associated with the PDMS thin film. Additionally, the need to prepare and cast electrodes is eliminated,

thereby reducing fabrication complexity. Through this proof of concept demonstration, we show that dielectrics under simple control can be used as valves in microfluidic systems.

Chapter 4: Conclusions and Future Work

4.1 Conclusions

In this thesis we focused on novel microfluidic applications. We reported a mixing methodology using passively controlled microswimmers and a valving technique utilizing the buckling instabilities of electroactive polymers.

In the first study, we demonstrated a simple technique to induce instantaneous microfluidic mixing using the magnetic tethering of artificially magnetized *P. multimicronucleatum*. Of the two magnetic configurations tested, the flat magnet orientation resulted in greater mixing due to the manner in which the paramecia were fixed in the microfluidic channel. Permanent magnets embedded in the microfluidic device passively controlled the motion of the microswimmers. Although the device is most similar to an active micromixer, no external power sources or artificial actuators were used.

In the second study, we reported a novel valving technique using the buckling instabilities of electroactive polymers. A geometrically confined thin film of PDMS under the influence of an externally applied high voltage signal deformed out-of-plane into a microfluidic channel. Electrolytic fluid solutions were used as the electrodes to provide optical inspection of valve functionality and ensure that applied voltages were not near the breakdown voltage of the PDMS thin film. This deformation resulted in the reduction of flow from an inlet stream in the main channel. The proof of concept of this technique is provided as the method requires refinement and further characterization.

4.2 Future Work

In this thesis we have demonstrated novel methods to mix fluids and regulate flow. In regards to the mixing experiment, more work needs to be done in the area of characterizing the magnetization of the paramecia, visualizing the mixing, and integrating components to filter out the paramecia from the mixed fluids. We also need to develop a method to observe the flow transience in the flat magnet scheme. This will allow us to further study how paramecia can be used to mix fluids and see the evolution of mixing in the main channel flow. Additionally, we need to quantify the nanoparticle uptake by the paramecia in order to determine the magnetization of the microorganisms. If we could effectively deciliate or immobilize the paramecia, we could use the Stokes drag formula to calculate the force the paramecia experience when in the presence of a permanent magnet. We could then devise a force balance between the magnetic force and drag experienced by paramecia to further tailor the flow parameters of the microfluidic experiment. We also should look into testing magnet configurations with different channel geometries to see if paramecia mix more effectively in a particular geometry. In order to develop this experiment into an applicable mixing technology, we would need to incorporate filtration techniques. We could also expand the type of fluids we mix to incorporate more biocompatible fluids to demonstrate the applicability of this microfluidic methodology. Although Chapter 2 details an experiment that is more developed than the proof of concept in Chapter 3, a great deal of work remains to be done to make this mixing technique an established method in the field of microfluidics.

In regards to the microvalve experiment, we need to finalize the design and fabrication protocols in order to obtain more data and statistically validate the method. We aim to develop a more reliable method to measure the film thickness and the other parameters needed to match

our experimental observations to theory. We need to quantify the flow rate through the microfluidic device. With a measurement of the flow rate, we can optimize our system to manipulate that flow rate and subsequently test the robustness of our design against others. This will demonstrate the usefulness of our device to various applications in microfluidics. Furthermore, we need to obtain a camera filter to help us obtain better images depicting valve operation. Once we have a better imaging method, we could include components that will aid us in characterizing the curvature of the film. By utilizing a high voltage monitor, we could further investigate thin film deformation with respect to the input voltage signal. If we could also devise a method to characterize the fluid force on the thin, dielectric membrane we would have a better understanding of what flow rates the device would be able to handle. Since this method is currently still being developed, we have a great deal of work ahead of us to develop this technology into a successful valving technology.

The future directions of work and goals laid out in this section are not complete. This section describes some of the work that needs to be done, but more work may become necessary while moving forward with these projects.

Appendix A: Microswimmer Mixing Experiment Using Microparticles

This section details an experiment similar to the flat magnet experiment performed in Chapter 2 with the substitution of fluorescent microparticles (Invitrogen F8819) and deionized water (ASTM Type II, LabChem Inc.) for the food coloring dyes. The purpose of this section is to show how paramecia are fixed in the flat magnet scheme. A stream of microparticles was introduced through one inlet while deionized water was introduced through the other inlet. These two streams joined in the main channel. The flow rate through the microfluidic device was 20 μL/hr. The microchannel was 300 by 100 μm. The Stokes number associated with the microparticles assures that the microparticles faithfully follow flow lines. Due to the nature of an inverted fluorescent microscopy setup, we were able to examine the flow under the magnet. This allowed us to see how the paramecia were fixed in the flat magnet experiment. During this specific experiment, the paramecia ingested microparticles and became large, glowing masses in the microchannel, thus making the microswimmers easily distinguishable from the microparticle stream in the microchannel. In order to show the nature of the flow without tethered paramecia, we captured images of the flow over time. The image panel in Figure A.1 shows that the flow in the microchannel is steady before paramecia are introduced. The flow profile shown in these images provides a basis for comparison for the case when paramecia are tethered in the microchannel.

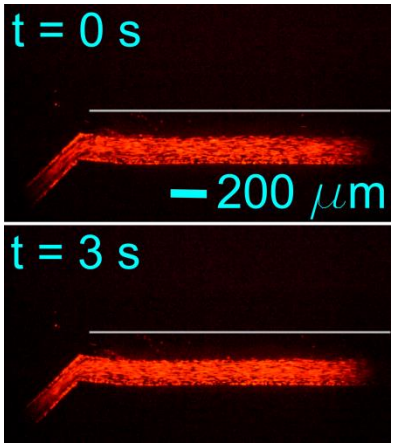

Figure A.1: Microchannel flow without tethered paramecia. As can be seen, over time the flow through the microchannel is steady. A gray line is provided to indicate the channel wall away from the microparticle stream. The Stokes number associated with the flow assures that the microparticles faithfully follow the streamlines of the flow.

The introduction of paramecia into the microchannel is given by Figure A.2.

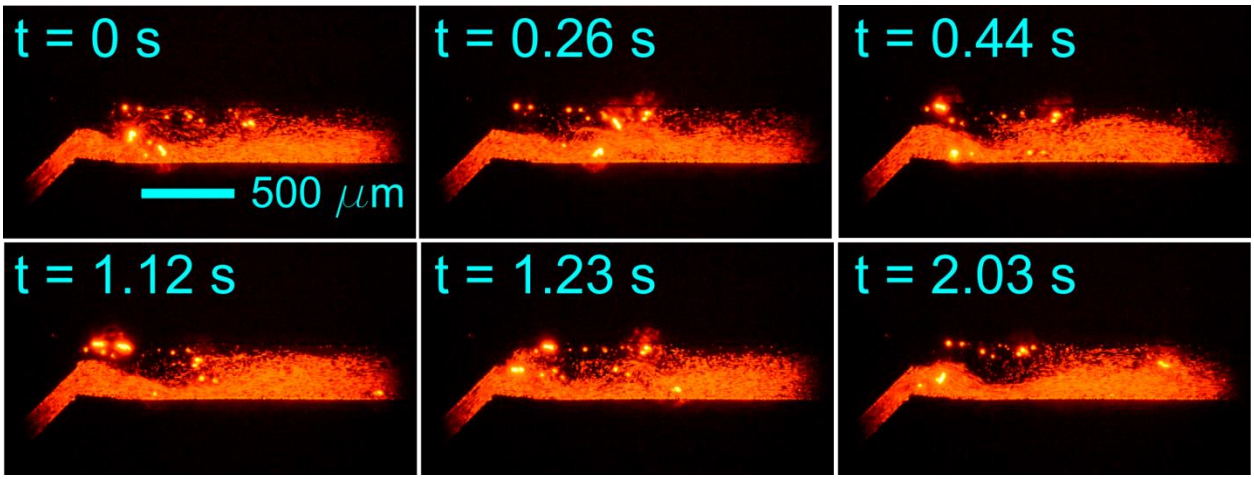

Figure A.2: Tethered paramecia position over time. This time series of images exhibits how paramecia are fixed in the microchannel while under the influence of the flat magnet orientation. From these images, we see that the paramecia move throughout the channel width and are effectively able to perturb the microparticle stream. The ciliary motion and bulk motion of the paramecia drive mixing between the microparticle and water streams. Microparticles faithfully follow the streamlines of the flow according to Stokes number.

From this figure, we are able to see that the paramecia are able to move across the channel width while locally fixed under the flat magnet orientation. The paramecia do not appear fixed against the channel walls as in the magnetic sandwich scheme. The ciliary and bulk movement of the microswimmers drives mixing between the microparticle and water streams by generating transverse flows to supplement diffusion. Although this specific experiment uses

microparticles to reveal the factors that induce mixing, we believe the same mechanisms causes mixing in the flat magnet test case presented in Chapter 2. We did not make any fundamental changes in the protocol to magnetize or tether the paramecia in the channel between this experiment and the flat magnet experiment with food dyes, and believe that the paramecia in both experiments should behave the same. As stated in Chapter 2, the manner in which the paramecia are fixed (as controlled by the magnet orientation) will determine how effective the microswimmers are at mixing two laminar streams, thus making the magnet orientation the main parameter between test cases.

In comparing the flow with and without paramecia, we are able to see that both are significantly different. The case without paramecia depicts a flow profile that is equally composed of a microparticle stream and water stream, while the case with paramecia depicts a disturbed flow profile in which the streams are not distinct. Using microparticles as flow indicators prevents meaningful quantitative analysis from being performed. The particles are not a continuous media and therefore the microparticles cannot accurately represent the flow since voids exist between particles in the images. Image analysis techniques would contain a great deal of noise due to the voids. Additionally, microparticles saturate the surrounding area. The saturation effect prevents us from distinguishing particle densities in space. Furthermore, mixing analyses cannot be performed since the streams cannot mix to form a different color.

Qualitatively, the flows in the cases provided in this section are different. The flow is steady in the case without paramecia and the flow is chaotic in the case with paramecia. This chaos is due to paramecia movement in the microchannel which is a function of the magnetic orientation.

References

1. Stone, H.A., A.D. Stroock, and A. Ajdari, *Engineering flows in small devices: Microfluidics toward a lab-on-a-chip.* Annu. Rev. Fluid Mech., 2004. **36**: p. 381-411.
2. Whitesides, G.M., *The origins and the future of microfluidics.* Nature, 2006. **442**(7101): p. 368-373.
3. Canny, M., *Flow and transport in plants.* Annual Review of Fluid Mechanics, 1977. **9**(1): p. 275-296.
4. Russel, W.B., D.A. Saville, and W.R. Schowalter, *Colloidal dispersions*. 1992: Cambridge University Press.
5. Manz, A., et al., *Planar chips technology for miniaturization and integration of separation techniques into monitoring systems: capillary electrophoresis on a chip.* Journal of Chromatography A, 1992. **593**(1): p. 253-258.
6. Stone, H. and S. Kim, *Microfluidics: basic issues, applications, and challenges.* AIChE Journal, 2001. **47**(6): p. 1250-1254.
7. Tüdős, A.J., G.A. Besselink, and R.B. Schasfoort, *Trends in miniaturized total analysis systems for point-of-care testing in clinical chemistry.* Lab Chip, 2001. **1**(2): p. 83-95.
8. Erickson, D. and D. Li, *Integrated microfluidic devices.* Analytica Chimica Acta, 2004. **507**(1): p. 11-26.
9. Hansen, C.L., et al., *A robust and scalable microfluidic metering method that allows protein crystal growth by free interface diffusion.* Proceedings of the National Academy of Sciences, 2002. **99**(26): p. 16531-16536.

10. Shim, J.-u., et al., *Using Microfluidics to Decouple Nucleation and Growth of Protein Crystals†.* Crystal Growth and Design, 2007. **7**(11): p. 2192-2194.

11. Dittrich, P.S. and A. Manz, *Lab-on-a-chip: microfluidics in drug discovery.* Nature Reviews Drug Discovery, 2006. **5**(3): p. 210-218.

12. Ramsey, R. and J. Ramsey, *Generating electrospray from microchip devices using electroosmotic pumping.* Analytical Chemistry, 1997. **69**(6): p. 1174-1178.

13. Xu, S., et al., *Generation of monodisperse particles by using microfluidics: control over size, shape, and composition.* Angewandte Chemie, 2005. **117**(5): p. 734-738.

14. Hardt, S., et al., *Passive micromixers for applications in the microreactor and μTAS fields.* Microfluidics and Nanofluidics, 2005. **1**(2): p. 108-118.

15. Nguyen, N.-T. and Z. Wu, *Micromixers—a review.* Journal of Micromechanics and Microengineering, 2005. **15**(2): p. R1.

16. Cho, B.S., et al., *Passively driven integrated microfluidic system for separation of motile sperm.* Analytical chemistry, 2003. **75**(7): p. 1671-1675.

17. Terry, S.C., J.H. Jerman, and J.B. Angell, *A gas chromatographic air analyzer fabricated on a silicon wafer.* Electron Devices, IEEE Transactions on, 1979. **26**(12): p. 1880-1886.

18. Goral, V.N., N.V. Zaytseva, and A.J. Baeumner, *Electrochemical microfluidic biosensor for the detection of nucleic acid sequences.* Lab on a Chip, 2006. **6**(3): p. 414-421.

19. Takamura, Y., et al., *Low-voltage electroosmosis pump for stand-alone microfluidics devices.* Electrophoresis, 2003. **24**(1-2): p. 185-192.

20. Oh, K.W. and C.H. Ahn, *A review of microvalves.* Journal of Micromechanics and Microengineering, 2006. **16**(5): p. R13.

21. Wang, S., et al., *Acoustically induced bubbles in a microfluidic channel for mixing enhancement.* Microfluidics and nanofluidics, 2009. **6**(6): p. 847-852.

22. Mao, X., et al., *Milliseconds microfluidic chaotic bubble mixer.* Microfluidics and Nanofluidics, 2010. **8**(1): p. 139-144.

23. Beebe, D.J., G.A. Mensing, and G.M. Walker, *Physics and applications of microfluidics in biology.* Annual review of biomedical engineering, 2002. **4**(1): p. 261-286.

24. Hessel, V., H. Löwe, and F. Schönfeld, *Micromixers—a review on passive and active mixing principles.* Chemical Engineering Science, 2005. **60**(8): p. 2479-2501.

25. Gobby, D., P. Angeli, and A. Gavriilidis, *Mixing characteristics of T-type microfluidic mixers.* Journal of Micromechanics and microengineering, 2001. **11**(2): p. 126.

26. Ottino, J.M., *The kinematics of mixing: stretching, chaos, and transport*. Vol. 3. 1989: Cambridge University Press.

27. Liau, A., et al., *Mixing crowded biological solutions in milliseconds.* Analytical chemistry, 2005. **77**(23): p. 7618-7625.

28. Stroock, A.D., et al., *Chaotic mixer for microchannels.* Science, 2002. **295**(5555): p. 647-651.

29. Liu, R.H., et al., *Passive mixing in a three-dimensional serpentine microchannel.* Microelectromechanical Systems, Journal of, 2000. **9**(2): p. 190-197.

30. Jones, S.W., O.M. Thomas, and H. Aref, *Chaotic advection by laminar flow in a twisted pipe.* Journal of Fluid Mechanics, 1989. **209**(1): p. 335-357.

31. Johnson, T.J. and L.E. Locascio, *Characterization and optimization of slanted well designs for microfluidic mixing under electroosmotic flow.* Lab on a Chip, 2002. **2**(3): p. 135-140.

32. Hessel, V., et al., *Laminar mixing in different interdigital micromixers: I. Experimental characterization.* AIChE Journal, 2003. **49**(3): p. 566-577.

33. Schönfeld, F., V. Hessel, and C. Hofmann, *An optimised split-and-recombine micro-mixer with uniform 'chaotic'mixing.* Lab Chip, 2004. **4**(1): p. 65-69.

34. Evans, J., D. Liepmann, and A.P. Pisano. *Planar laminar mixer*. in *Proc. MEMS'97, 10th IEEE Int. Workshop Micro Electromechanical System (Nagoya, Japan)*. 1997.

35. Bau, H.H., J. Zhong, and M. Yi, *A minute magneto hydro dynamic (MHD) mixer*. Sensors and Actuators B: Chemical, 2001. **79**(2): p. 207-215.

36. Yang, Z., et al., *Active micromixer for microfluidic systems using lead-zirconate-titanate (PZT)-generated ultrasonic vibration.* Electrophoresis, 2000. **21**(1): p. 116-119.

37. Yang, Z., et al., *Ultrasonic micromixer for microfluidic systems.* Sensors and Actuators A: Physical, 2001. **93**(3): p. 266-272.

38. Liu, R.H., et al., *Bubble-induced acoustic micromixing.* Lab on a Chip, 2002. **2**(3): p. 151-157.

39. Glasgow, I. and N. Aubry, *Enhancement of microfluidic mixing using time pulsing.* Lab on a Chip, 2003. **3**(2): p. 114-120.

40. El Moctar, A.O., N. Aubry, and J. Batton, *Electro-hydrodynamic micro-fluidic mixer.* Lab Chip, 2003. **3**(4): p. 273-280.

41. Oddy, M., J. Santiago, and J. Mikkelsen, *Electrokinetic instability micromixing.* Analytical Chemistry, 2001. **73**(24): p. 5822-5832.

42. Sato, K. and M. Shikida, *An electrostatically actuated gas valve with an S-shaped film element.* Journal of Micromechanics and Microengineering, 1994. **4**(4): p. 205.

43. Li, H., et al., *Fabrication of a high frequency piezoelectric microvalve.* Sensors and Actuators A: Physical, 2004. **111**(1): p. 51-56.

44. Jerman, H. *Electrically-activated, normally-closed diaphragm valves*. in *Solid-State Sensors and Actuators, 1991. Digest of Technical Papers, TRANSDUCERS'91., 1991 International Conference on*. 1991. IEEE.

45. Lisec, T., M. Kreutzer, and B. Wagner, *A bistable pneumatic microswitch for driving fluidic components.* Sensors and Actuators A: Physical, 1996. **54**(1): p. 746-749.

46. Bae, B., et al., *Feasibility test of an electromagnetically driven valve actuator for glaucoma treatment.* Microelectromechanical Systems, Journal of, 2002. **11**(4): p. 344-354.

47. Goll, C., et al., *An electrostatically actuated polymer microvalve equipped with a movable membrane electrode.* Journal of Micromechanics and Microengineering, 1997. **7**(3): p. 224.

48. Robertson, J. and K.D. Wise, *A low pressure micromachined flow modulator.* Sensors and Actuators A: Physical, 1998. **71**(1): p. 98-106.

49. Shikida, M., et al., *Electrostatically driven gas valve with high conductance.* Microelectromechanical Systems, Journal of, 1994. **3**(2): p. 76-80.

50. Schaible, J., et al. *Electrostatic microvalves in silicon with 2-way-function for industrial applications*. in *Proceedings transducers*. 2001.

51. van der Wijngaart, W., et al., *A high-stroke, high-pressure electrostatic actuator for valve applications.* Sensors and Actuators A: Physical, 2002. **100**(2): p. 264-271.

52. Rogge, T., Z. Rummler, and W. Schomburg, *Polymer micro valve with a hydraulic piezo-drive fabricated by the AMANDA process.* Sensors and Actuators A: Physical, 2004. **110**(1): p. 206-212.

53. Shao, P., Z. Rummler, and W.K. Schomburg, *Polymer micro piezo valve with a small dead volume.* Journal of Micromechanics and Microengineering, 2004. **14**(2): p. 305.

54. Barth, P.W. *Silicon microvalves for gas flow control*. in *The 1995 8 th International Conference on Solid-State Sensors and Actuators, and Eurosensors IX. Part 2(of 2)*. 1995.

55. Takao, H., et al., *A MEMS microvalve with PDMS diaphragm and two-chamber configuration of thermo-pneumatic actuator for integrated blood test system on silicon.* Sensors and Actuators A: Physical, 2005. **119**(2): p. 468-475.

56. Wolf, R.H. and A.H. Heuer, *TiNi (shape memory) films silicon for MEMS applications.* Microelectromechanical Systems, Journal of, 1995. **4**(4): p. 206-212.

57. Kohl, M., K. Skrobanek, and S. Miyazaki, *Development of stress-optimised shape memory microvalves.* Sensors and Actuators A: Physical, 1999. **72**(3): p. 243-250.

58. Kahn, H., M. Huff, and A. Heuer, *The TiNi shape-memory alloy and its applications for MEMS.* Journal of Micromechanics and Microengineering, 1998. **8**(3): p. 213.

59. Schomburg, W. and C. Goll, *Design optimization of bistable microdiaphragm valves.* Sensors and Actuators A: Physical, 1998. **64**(3): p. 259-264.

60. Oh, K.W., et al., *World-to-chip microfluidic interface with built-in valves for multichamber chip-based PCR assays.* Lab Chip, 2005. **5**(8): p. 845-850.

61. Hasegawa, T., et al., *Multi-directional micro-switching valve chip with rotary mechanism.* Sensors and Actuators A: Physical, 2008. **143**(2): p. 390-398.

62. Go, J.S. and S. Shoji, *A disposable, dead volume-free and leak-free in-plane PDMS microvalve.* Sensors and Actuators A: Physical, 2004. **114**(2): p. 438-444.

63. Lagally, E.T., P.C. Simpson, and R.A. Mathies, *Monolithic integrated microfluidic DNA amplification and capillary electrophoresis analysis system.* Sensors and Actuators B: Chemical, 2000. **63**(3): p. 138-146.

64. Takao, H., M. Ishida, and K. Sawada. *A pneumaticallyactuated silicon microvalve and its application to functional fluidic integrated circuits*. in *Tech. Dig. Papers 11th Int. Conf. on Solid-State Sensors and Actuators (Transducers' 01)*. 2001.

65. Unger, M.A., et al., *Monolithic microfabricated valves and pumps by multilayer soft lithography.* Science, 2000. **288**(5463): p. 113-116.

66. Liu, J., C. Hansen, and S.R. Quake, *Solving the "world-to-chip" interface problem with a microfluidic matrix.* Analytical chemistry, 2003. **75**(18): p. 4718-4723.

67. Chou, H.-P., et al., *A microfabricated device for sizing and sorting DNA molecules.* Proceedings of the National Academy of Sciences, 1999. **96**(1): p. 11-13.

68. Sleigh, M.A., *Cilia and flagella*. 1974: Academic Press.

69. Jana, S., S.H. Um, and S. Jung, *Paramecium swimming in capillary tube.* Physics of Fluids, 2012. **24**: p. 041901.

70. Kim, J., et al., *Mixing enhancement by biologically inspired convection in a micro-chamber using alternating current galvanotactic control of the Tetrahymena pyriformis.* Applied Physics Letters, 2013. **103**(10): p. 103703-103703-4.

71. Hyung Kim, D., et al., *Three-dimensional control of Tetrahymena pyriformis using artificial magnetotaxis.* Applied Physics Letters, 2012. **100**(5): p. 053702-053702-3.

72. Van Houten, J., *Two mechanisms of chemotaxis inParamecium.* Journal of comparative physiology, 1978. **127**(2): p. 167-174.

73. Kim, D.H., et al., *Artificial magnetotactic motion control of Tetrahymena pyriformis using ferromagnetic nanoparticles: A tool for fabrication of microbiorobots.* Applied Physics Letters, 2010. **97**(17): p. 173702-173702-3.

74. Itoh, A., *Motion control of protozoa for bio-MEMS.* Mechatronics, IEEE/ASME Transactions on, 2000. **5**(2): p. 181-188.

75. Brown, F.A., *Responses of the planarian, Dugesia, and the protozoan, Paramecium, to very weak horizontal magnetic fields.* The Biological Bulletin, 1962. **123**(2): p. 264-281.

76. Guevorkian, K. and J.M. Valles, *In situ imaging of micro-organisms in intense magnetic fields.* Review of scientific instruments, 2005. **76**(10): p. 103706-103706-3.

77. Guevorkian, K. and J.M. Valles, *Swimming Paramecium in magnetically simulated enhanced, reduced, and inverted gravity environments.* Proceedings of the National Academy of Sciences, 2006. **103**(35): p. 13051-13056.

78. Guevorkian, K. and J.M. Valles, *Aligning< i> Paramecium caudatum</i> with Static Magnetic Fields.* Biophysical journal, 2006. **90**(8): p. 3004-3011.

79. Roberts, A., *Motion of< i> Paramecium</i> in static electric and magnetic fields.* Journal of Theoretical Biology, 1970. **27**(1): p. 97-106.

80. Fahrni, F., M.W.J. Prins, and L.J. van IJzendoorn, *Micro-fluidic actuation using magnetic artificial cilia.* Lab Chip, 2009. **9**(23): p. 3413-3421.

81. den Toonder, J., et al., *Artificial cilia for active micro-fluidic mixing.* Lab on a Chip, 2008. **8**(4): p. 533-541.

82. Khatavkar, V.V., et al., *Active micromixer based on artificial cilia.* Physics of Fluids, 2007. **19**(8): p. 083605-083605-13.

83. Massart, R., *Preparation of aqueous magnetic liquids in alkaline and acidic media.* IEEE Transactions on Magnetics 1981. **17**(2): p. 1247-1248.

84. Bajaj, A., et al., *Stability, toxicity and differential cellular uptake of protein passivated-Fe3O4 nanoparticles.* Journal of Materials Chemistry, 2009. **19**(35): p. 6328-6331.

85. Garstecki, P., et al., *Mixing with bubbles: a practical technology for use with portable microfluidic devices.* Lab Chip, 2005. **6**(2): p. 207-212.

86. Carpi, F., S. Bauer, and D. De Rossi, *Stretching dielectric elastomer performance.* Science, 2010. **330**(6012): p. 1759-1761.

87. Dubois, P., et al., *Microactuators based on ion implanted dielectric electroactive polymer (EAP) membranes.* Sensors and actuators A: Physical, 2006. **130**: p. 147-154.

88. OHalloran, A., F. OMalley, and P. McHugh, *A review on dielectric elastomer actuators, technology, applications, and challenges.* Journal of Applied Physics, 2008. **104**(7): p. 071101-071101-10.

89. Goulbourne, N., et al. *Modeling of a dielectric elastomer diaphragm for a prosthetic blood pump*. in *Smart structures and Materials*. 2003. International Society for Optics and Photonics.

90. Pelrine, R., et al., *High-speed electrically actuated elastomers with strain greater than 100%.* Science, 2000. **287**(5454): p. 836-839.

91. Brochu, P. and Q. Pei, *Advances in dielectric elastomers for actuators and artificial muscles.* Macromolecular rapid communications, 2010. **31**(1): p. 10-36.

92. Carpi, F., et al., *Dielectric elastomers as electromechanical transducers: Fundamentals, materials, devices, models and applications of an emerging electroactive polymer technology*. 2011: Elsevier.

93. Lide, D.R., *CRC Handbook of Chemistry and Physics 1999-2000: A Ready-Reference Book of Chemical and Physical Data (CRC Handbook of Chemistry and Physics*. 1998, CRC Press, Boca Raton, Florida, USA.